

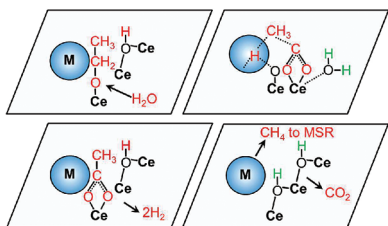
Production of Hydrogen from Ethanol: Review of Reaction Mechanism and Catalyst Deactivation

Lisiane V. Mattos,[†] Gary Jacobs,[‡] Burtron H. Davis,[‡] and Fábio B. Noronha^{*,§}

[†]Departamento de Engenharia Química e de Petróleo, Universidade Federal Fluminense (UFF), Rua Passo da Pátria, 156-CEP 24210-240, Niterói, RJ, Brazil

[‡]Center for Applied Energy Research, The University of Kentucky, 2540 Research Park Drive, Lexington, Kentucky 40511, United States

[§]Instituto Nacional de Tecnologia—INT, Av. Venezuela 82, CEP 20081-312, Rio de Janeiro, Brazil



CONTENTS

1. Introduction	4094
2. Reaction Mechanisms	4095
2.1. Catalytic Tests	4095
2.1.1. Reaction Pathways Network	4095
2.1.2. Effect of Reaction Conditions and Choice of Catalyst on the Reaction Pathway	4095
2.1.3. Reaction Mechanism in Aqueous-Phase Reforming and Reforming in Supercritical Water	4095
2.2. Spectroscopic and Thermal Desorption Studies	4098
2.2.1. Fundamental Mechanistic Studies on Transition Metal Surfaces	4099
2.2.2. Oxygenate Reaction Pathways on Oxides and Supported Metal Catalysts	4099
2.2.3. Obtaining Mechanistic Information under Reaction Conditions	4100
2.3. General Overview	4103
3. Catalyst Deactivation	4105
3.1. Carbon Deposition	4106
3.1.1. Reaction Pathways for Carbon Formation	4107
3.1.2. Nature of the Carbon Formed	4107
3.1.3. Effect of Ethanol Purity on Carbon Formation (Bioethanol)	4108
3.1.4. Strategies for Minimizing Carbon Formation	4112
3.2. Metal Sintering	4112
3.3. Metal Oxidation	4116
3.4. General Overview	4117
4. Conclusions and Suggested Path Forward	4117
Author Information	4118
Corresponding Author	4119
Biographies	4119
Acknowledgments	4120
References	4120

1. INTRODUCTION

The light alcohol ethanol is an important candidate as a chemical carrier of hydrogen, the production of which is useful in a range of fuel cell applications. Not only is it less hazardous than methanol but it can be produced from a variety of biomass sources. Its use could conceivably lead to a decrease in CO₂ emissions. Currently, bioethanol is produced by the fermentation of sugar cane, corn grains, and other starch-rich materials, and is considered to be a mature technology. Recent research has focused on producing bioethanol from lignocellulosic biomass, the so-called second-generation bioethanol. Ethanol production from lignocellulose would open up the possibility for the utilization of diverse and low-cost biomass, such as agricultural wastes and forestry residues (e.g., straw, grasses, corn stover, and wood); in this way, food could be produced along with bioethanol from agricultural sources.¹

As demonstrated by recent reviews, hydrogen production via the catalytic steam reforming (SR) of ethanol has been extensively studied.^{2–5} These reviews summarize the current status of this technology. They include the chemical processes for hydrogen production (e.g., SR, water gas shift (WGS), preferential oxidation of CO (PROX), and methanation), reaction conditions, catalysts (e.g., oxide and oxide-supported metal catalysts), and the thermodynamics of the SR of ethanol. However, to date, there has not been a review dedicated to either defining the reaction mechanism of SR of ethanol or to delineating the routes of catalyst deactivation during reaction. This review aims at summarizing various mechanistic features of ethanol reforming, not only to assess the current state of the art in the field but also to distill recent insights that could shed light on a path forward for improving catalyst design.

At the heart of catalytic reforming reactions is the surface mechanism. Over the past decade, good progress has been made in developing an understanding regarding surface reaction pathways, as well as harnessing the most likely intermediates involved in the catalysis of metals, metal oxides, and, most recently, novel bifunctional catalysts that rely on interfaces formed between a metal and an active oxide. This review begins by summarizing these findings. Research has focused on temperature-programmed desorption and infrared

Received: January 6, 2011

Published: May 23, 2012

spectroscopic investigations. The discussion of the mechanism ends by presenting a number of specific case studies to not only demonstrate the power of infrared spectroscopy for studying ethanol reforming catalysts but also show precisely what kinds of information can be gleaned using this technique.

Although an understanding of the fundamental mechanism is important, currently the greatest challenge in developing new catalysts is improvement in catalyst stability. Section 3 examines the many different ways that carbon deposits can form during ethanol reforming. This challenging problem arises as a result of C–C bond scission in the ethanol molecule; this is not encountered with methanol. The nature of the carbonaceous deposits depends on both the type of metal present (e.g., base metal or noble metal) and the reaction conditions used (e.g., feed composition and temperature). Many recent investigations have focused on applying different strategies to either hinder carbon formation or to react it from the surface. Five of these strategies will be discussed in detail. These include modifications to the catalyst itself (e.g., adding active oxide components), as well as adjusting feed ratios to favor carbon removal from the surface (e.g., cofeeding O₂). In addition to carbon formation, other sources of catalyst deactivation such as oxidation state changes in the catalyst, as well as the sintering of active surfaces, are considered.

On the basis of a critical review of the recent literature, some possibilities regarding future directions for the improvement of ethanol reforming catalyst formulations and processes will then be offered. Overall, the hope is to move us closer to making the commercial use of bioethanol as a chemical carrier for hydrogen a reality.

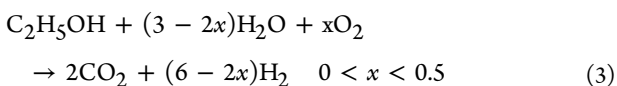
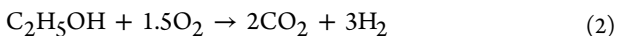
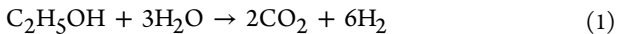
2. REACTION MECHANISMS

A number of different approaches have been undertaken to shed light on the surface catalytic mechanisms involved in ethanol conversion reactions. This review highlights insights obtained from catalytic testing results, spectroscopic methods, and thermal desorption techniques. These will now be discussed in greater detail.

2.1. Catalytic Tests

2.1.1. Reaction Pathways Network. Several studies aimed at identifying the reaction pathways taking place in ethanol conversion reactions are based on a detailed analysis of the final products obtained during catalytic testing. The result of these efforts is that a number of mechanistic schemes have been proposed in the literature.^{2–5}

Typical routes for hydrogen production from ethanol are shown in the following equations: SR (eq 1); partial oxidation (POX) (eq 2); and oxidative steam reforming (OSR) (eq 3).

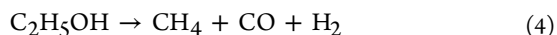


Although the SR of ethanol provides a high hydrogen yield, it is a highly endothermic reaction, and therefore, high operation temperatures are necessary. The POX of ethanol is an exothermic reaction that exhibits fast start-up and response times, both of which are critically important for vehicle fuel cell applications. Furthermore, the POX reactor is more compact than that of a steam reformer. This is due to the fact that this reaction does not require the indirect addition of heat via a heat exchanger. There are, however, some drawbacks that include

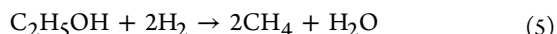
difficulty in controlling the reaction due to hot-spot formation and low hydrogen yields. The OSR of ethanol combines both the SR and POX reactions. This means that their relative rates can be adjusted to achieve thermally neutral operating conditions (i.e., autothermal reforming). This may preclude the need for an external heat supply, depending on the water and oxygen contents of the feed.⁶

However, many other reactions can occur simultaneously with hydrogen production reactions (eqs 1–3). Some of these lead to the formation of undesirable products.^{2–5} The reaction network can, for example, include

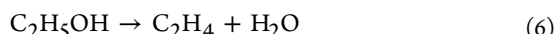
- Ethanol decomposition (ED) to CH₄, CO, and H₂:



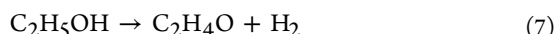
- Ethanol hydrogenolysis to CH₄ and H₂O:



- Ethanol dehydration to ethylene:



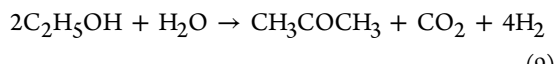
- Ethanol dehydrogenation to acetaldehyde:



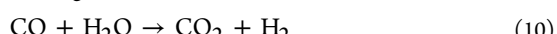
- Acetaldehyde decomposition to CH₄ and CO:



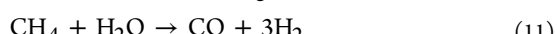
- Acetone formation via aldolic condensation, followed by dehydrogenation:



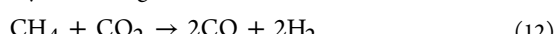
- Water gas shift (WGS):



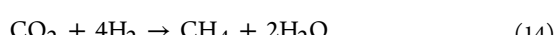
- Methane steam reforming:



- Dry reforming of methane:



- Methanation:



The relative importance of each of these reaction pathways depends on both the reaction conditions selected (e.g., reaction temperature, feed composition, and residence time) and the choice of catalyst. In the literature, there are many thermodynamic^{7–13} and experimental^{14–40} studies evaluating the effect of process variables (e.g., reaction temperature, pressure, water-to-ethanol molar ratio and oxygen-to-ethanol molar ratio) on the product distributions of SR, POX, and OSR of ethanol. The influence of reaction conditions and the nature of the catalyst will now be briefly described.

2.1.2. Effect of Reaction Conditions and Choice of Catalyst on the Reaction Pathway. The reaction temperature significantly affects both the the activity and product distribution for the conversion of ethanol using SR, POX, and OSR reactions.^{14–31} The calculation of the thermodynamic equilibrium composition for these three reactions reveals that hydrogen, CO, CO₂, and methane are the main products^{7–13} (Figure 1). As the temperature is raised, methane and CO₂

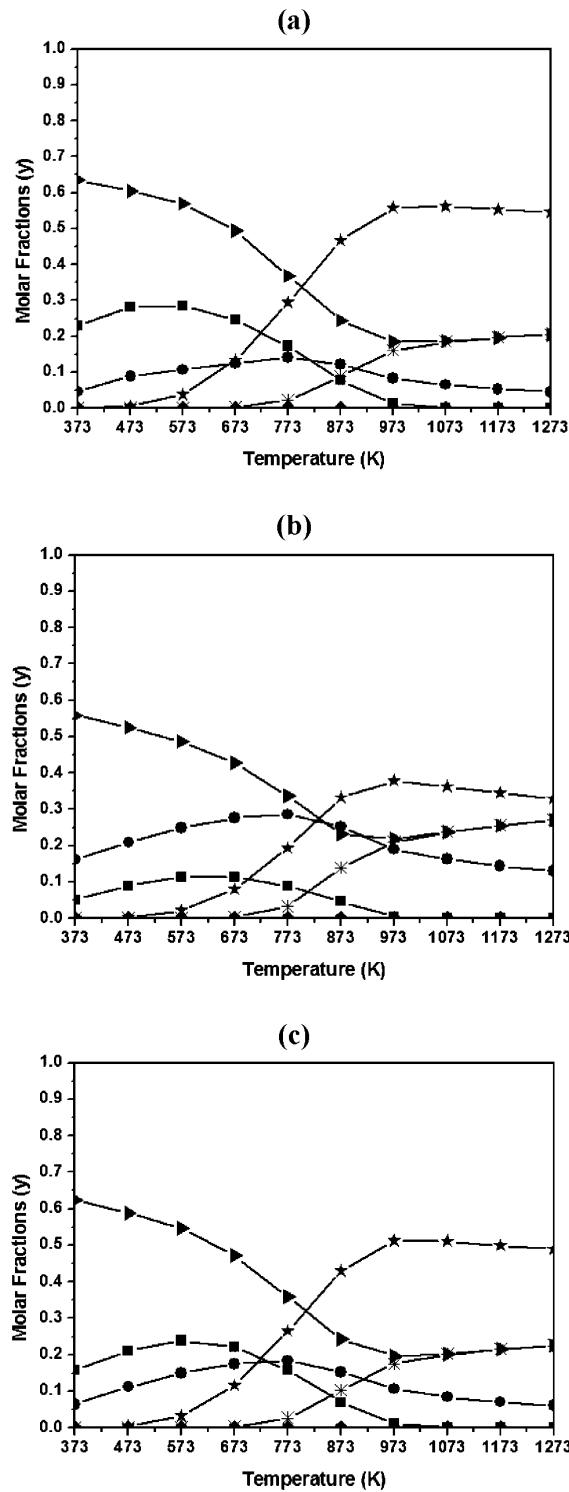


Figure 1. Product distributions versus reaction temperature for (a) SR of ethanol with water-to-ethanol molar ratio of 3.0; (b) POX of ethanol with oxygen-to-ethanol molar ratio of 0.5; (c) OSR of ethanol with water-to-ethanol molar ratio of 2.0 and oxygen-to-ethanol molar ratio of 0.5: (■) CH_4 , (●) CO_2 , (*) CO , (star) H_2 , (▲) H_2O , (○) O_2 , (◆) ethanol.

concentrations decrease, whereas those of hydrogen and CO increase. Acetaldehyde, ethylene, and acetone are not predicted to be present at equilibrium. This indicates that they are not thermodynamically stable products. In practice, at low reaction temperatures, a wide range of undesirable byproducts such as

oxygenated compounds (e.g., acetaldehyde and acetone) as well as hydrocarbons (e.g., ethylene) are also detected.^{14–31} This suggests that, under these conditions, reforming reactions are kinetically controlled.¹² In fact, ethanol dehydrogenation and dehydration reactions are faster than the steam reforming reaction, and hence, acetaldehyde and ethylene can be present in significant concentrations in the product distribution. Increasing the reaction temperature leads to an increase in ethanol conversion. This is accompanied by a concomitant decrease in the selectivities of acetaldehyde, acetone, and ethylene and increases in those of H_2 , CO , CO_2 , and CH_4 . At higher temperatures, acetaldehyde, acetone, and ethylene are no longer detected and the formation of H_2 and CO is thermodynamically favored. The temperature range where changes in catalytic activity and product selectivities are observed depends on the nature of the catalyst (i.e., support and metal) and the reaction conditions used (i.e., H_2O -to-ethanol molar ratio, O_2 -to-ethanol molar ratio, and residence time).

Fatsikotas et al.^{14,15} investigated the performance of $\text{Ni}/\text{Al}_2\text{O}_3$, $\text{Ni}/\text{La}_2\text{O}_3$, and $\text{Ni}/(\text{La}_2\text{O}_3/\text{Al}_2\text{O}_3)$ catalysts (20 wt % of Ni) for the SR of ethanol at different temperatures using the temperature-programmed surface reaction (TPSR) technique. At temperatures lower than 473 K, for La_2O_3 -supported Ni catalyst, ethanol conversion was very low and the main products observed were acetaldehyde and hydrogen (Figure 2). The formation of these

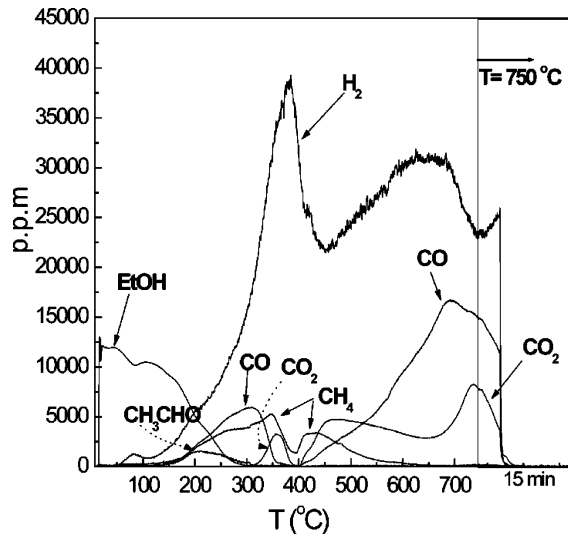


Figure 2. Temperature-programmed reaction over 20% $\text{Ni}/\text{La}_2\text{O}_3$. A mixture containing 1% EtOH and 2% H_2O in He was flowed ($44 \text{ cm}^3/\text{min}^{-1}$) while the temperature was ramped at a linear rate of 15 K min^{-1} ; mass of catalyst, 100 mg; $P = 1 \text{ atm}$. Reprinted with permission from ref 15. Copyright 2004 Elsevier.

products was attributed to the ethanol dehydrogenation reaction (eq 7). The fact that no ethylene was detected indicates that ethanol dehydration (eq 6) was disfavored using the $\text{Ni}/\text{La}_2\text{O}_3$ catalyst. This result was explained by a lack of suitable acidic sites on the La_2O_3 support. Increasing the reaction temperature from 473 to 623 K increased the production of H_2 , CO, CO_2 , and CH_4 and reduced the formation of acetaldehyde. At 623 K, ethanol conversion was complete and acetaldehyde was no longer detected. The increases in H_2 and CO_2 formation were ascribed to the SR of both ethanol and acetaldehyde. Moreover, the production of CO_2 and CH_4 implied participation by the WGS (eq 10) and methanation (eq 13 and 14) reactions, respectively.

At temperatures higher than 623 K, the selectivities to H₂ and CO increased. The simultaneous decreases in CO₂ and CH₄ selectivities observed were attributed to both the steam reforming and dry reforming of CH₄ (eqs 11 and 12). These reactions are thermodynamically favored at high temperatures.

The amount of water and the presence/absence of oxygen in the feed also influences ethanol conversion and product distribution obtained for ethanol reforming reactions using different catalysts.^{6–13,15–18,23,31–40} In the literature, the influence of the H₂O-to-ethanol molar ratio on the performance of different catalysts for SR of ethanol has been investigated extensively.^{7–10,12,16–18,22,23,29,35,37–39} The SR of ethanol has been carried out using H₂O-to-ethanol molar ratios ranging from 1.0 to 15.0. In general, increasing the H₂O-to-ethanol molar ratio is found to increase the conversion of ethanol. With respect to product distribution, it is seen that, by increasing the amount of water in the feed, the production of H₂ and CO₂ also increased and the rate of CO formation decreased. This indicates that the addition of water promotes the SR of ethanol and/or the WGS reaction. Furthermore, data indicate that increasing the H₂O-to-ethanol molar ratio was found to decrease the rates of formation of byproduct such as ethylene and acetaldehyde. The addition of water shifts the equilibrium of the dehydration reaction to favor the reactants and promotes the acetaldehyde decomposition reaction. However, the addition of large amounts of water implies higher operating costs for ethanol vaporization, which must be taken into account.

Some authors also evaluated the effect of oxygen addition to the feed for the ethanol reforming reactions.^{11–13,17–20,32,35} Depending on the O₂-to-ethanol molar ratio, the partial and total oxidation reactions (eqs 15 and 16) can also occur. This alters the product distribution:³⁴

- Incomplete oxidation of ethanol:



- Total oxidation of ethanol:

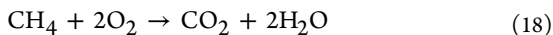


Additional oxidation reactions that may also occur in the presence of oxygen in the feed are as follows:⁵

- CO combustion:



- Methane combustion:



- Dehydrogenative oxidation of ethanol:



The presence of oxygen in the feed increased the initial ethanol conversion for all the catalysts studied but had a deleterious impact on H₂ selectivity. Furthermore, the CO₂ formation rate increased; this is most likely due to the ethanol combustion reaction (eq 16). Moreover, because the presence of oxygen was found to increase the production of acetaldehyde, it can be concluded that oxygen promotes the dehydrogenation of ethanol to acetaldehyde (eq 19).

However, in spite of the large number of investigations about ethanol conversion reactions that are found in the literature, those that provide comparisons of the SR, POX, and OSR of ethanol reactions are scarce.^{6,17,36–38} de Lima et al.^{37,38} studied the effect of feed composition during the ethanol reforming

reactions (ED, POX, SR, and OSR of ethanol) over 1.5 wt % Pt/CeZrO₂ and 10 wt % Co/CeO₂ catalysts at 773 K. The reactions were performed at different H₂O-to-ethanol molar ratios (for Pt/CeZrO₂:H₂O/ethanol = 2.0–5.0 and for Co/CeO₂:H₂O/ethanol = 3.0 and 10.0) and an O₂-to-ethanol molar ratio of 0.5. For both catalysts, the addition of water, oxygen, or both to the ethanol feed increased the conversion of ethanol, suggesting that these molecules promote the surface reaction. Regarding product distributions, increasing the concentration of water in the feed increased H₂ and CO₂ production but decreased the CO formation rate. According to the authors, adding water favored the WGS reaction. Furthermore, increasing the H₂O-to-ethanol molar ratio decreased both acetaldehyde and ethylene formation rates. Water inhibits the dehydration of ethanol but apparently facilitates the decomposition of acetaldehyde formed. Oxygen addition likely oxidized a fraction of hydrogen to water, as a decrease in H₂ selectivity was observed. Likewise, an increase in CO₂ selectivity indicated that it promotes ethanol combustion as well.

Several research groups^{14–16,21,23,25,41,42} investigated the effect of the residence time on the SR of ethanol. Decreasing the residence time decreased the conversion of ethanol as well as selectivities to H₂ and CO. On the other hand, as residence time decreased, the production of byproducts (e.g., acetaldehyde, ethylene) increased. According to the authors, the ethylene and acetaldehyde reforming reactions did not occur at low residence times. This implies that acetaldehyde is very likely an important intermediate in the SR pathway.

Both the nature of the metal and the support significantly affect the product distribution. Different catalysts, including metal oxides, mixed metal oxides, supported base metals (Ni, Co, Cu), and supported noble metals (Pd, Pt, Rh, Ru, Ir), have all been extensively studied for the SR, POX, and OSR reactions.^{2–5} However, only a few papers compare the performance of catalysts containing different metals dispersed over the same support.^{21,43–46} Liguras et al.²¹ investigated the SR of ethanol at high temperature (650–800 °C) over Pd/Al₂O₃ (1 wt % Pd), Pt/Al₂O₃ (1 wt % Pt), Rh/Al₂O₃ (0.5, 1.0, and 2.0 wt % Rh), and Ru/Al₂O₃ (1.0, 3.0, and 5.0 wt % Ru). As shown in Figure 3, Rh was found to be significantly more selective to H₂ and CO. The following order was observed: Rh > Pt > Ru ≈ Pd. Acetaldehyde selectivity followed the reverse order. These results were attributed to the high reforming capability of Rh. A highly loaded Ru catalyst exhibited a comparable selectivity to that of the Rh catalyst. Aufprêtre et al.⁴³ studied the effect of the nature of the metal on the SR of ethanol reaction. Different catalysts were tested: 1 wt % Rh/Al₂O₃, 1 wt % Pt/Al₂O₃, 0.75 wt % Pd/Al₂O₃, 0.67 wt % Pt/Al₂O₃, 9.7 wt % Ni/Al₂O₃, 9.1 wt % Cu/Al₂O₃, 9.8 wt % Zn/Al₂O₃, and 8.7 wt % Fe/Al₂O₃. Rh- and Ni-based catalysts showed the highest H₂ and CO₂ selectivities. Frusteri et al.⁴⁴ studied the performance of 3 wt % Rh/MgO, 3 wt % Pd/MgO, 21 wt % Ni/MgO, and 21 wt % Co/MgO catalysts for the SR of ethanol. Rh-, Ni-, and Co-based catalysts exhibited similar product distributions characterized mainly by H₂, CO₂, and CO. Ni/MgO displayed the highest H₂ selectivity. Furthermore, the use of Rh showed significant formation of methane. This was attributed to its lower activity for the SR of methane compared to Ni and Co. The Pd/MgO catalyst exhibited the highest methane selectivity, and ethylene and acetaldehyde were formed in significant amounts. The selectivity to methane decreased whereas the formation of acetaldehyde increased during the reaction, which suggests that Pd loses its activity for acetaldehyde decomposition,

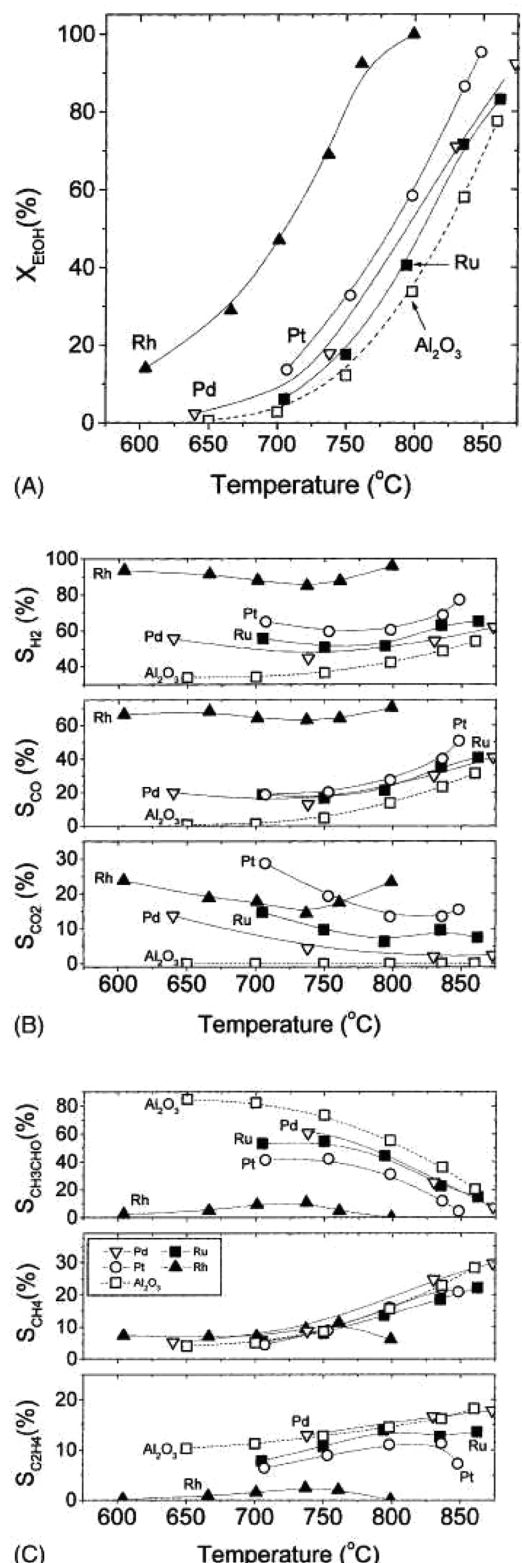


Figure 3. Effect of reaction temperature on the conversion of ethanol (A) and on the selectivities toward reaction products (B and C) obtained over 1% Me/Al₂O₃ catalysts (Me = Pd, Ru, Pt, Rh) and the Al₂O₃ support. Reprinted with permission from ref 21. Copyright 2003 Elsevier.

probably due to carbon formation. Basagiannis et al.⁴⁵ carried out the SR of ethanol at low temperature (300–450 °C) over 0.5 wt % Pt/Al₂O₃, 1 wt % Pd/Al₂O₃, 2 wt % Rh/Al₂O₃, and 5 wt % Ru/Al₂O₃. Under these reaction conditions, the main

products observed were H₂, CO, CO₂, methane, acetaldehyde, and ethylene. These were attributed to ethanol dehydrogenation to acetaldehyde (eq 7), ethanol and/or acetaldehyde decomposition (eqs 4 and 8), ethanol dehydration to ethylene (eq 6), and WGS (eq 10) reactions. Although Rh exhibited the highest selectivity to H₂, Ru on the other hand favored the formation of acetaldehyde. Methane selectivity varied in the following order: Pd ≈ Pt > Rh ≫ Ru. Recently, combinatorial tools and high-throughput experimentation techniques have been used to design catalysts for low-temperature SR of ethanol.^{47,48} In one of these studies,⁴⁸ five supports (Al₂O₃, SiO₂, TiO₂, CeO₂, and ZrO₂) and 42 metals having 4 different loadings (0.5, 1, 2.5, and 5 wt %) were evaluated for the SR of ethanol at 300 °C. A water-to-ethanol molar ratio of 6 was used. The only metals found to be active for ethanol conversion were those corresponding to groups VIII and IB of the periodic table. The amount of hydrogen formed decreased in the following order: Pt > Rh ≫ Pd > Co, Ni, Cu, Ir. The highest production rate of H₂ was observed for the 5 wt % Pt/CeO₂ catalyst.

However, the nature of the metal and its influence on the different reaction pathways are still not well-established. This appears to be mainly due to difficulties in distinguishing between apparent and real effects. In fact, there are numerous factors that can also affect the product distribution: (i) ethanol conversion, (ii) metal dispersion, and (iii) the nature of the support. For example, acetaldehyde is an important intermediate formed during the ethanol dehydrogenation reaction. By increasing the conversion, acetaldehyde may further react, producing H₂, CO, and methane. Therefore, depending on the level of ethanol conversion, different products may be formed. Because the majority of papers did not compare the product selectivity at the same conversion level, this can lead to misleading conclusions. In addition, the metal dispersion is directly related to ethanol conversion and, consequently, impacts the product distribution. Generally, comparisons between product distributions using different catalysts did not take into account the different metal dispersions. Finally, one additional complication is that most of the metal oxides used as catalyst supports exhibit activity for the SR reaction. In spite of their lower activity relative to supported metal catalysts, a wide range of undesirable byproducts (e.g., ethylene, acetaldehyde, and acetone) are formed during SR of ethanol over metal oxides compared to supported metal catalysts. Ultimately, this depends on the surface properties of the metal oxide. Therefore, the careful elimination of these artifacts is fundamentally important in order to understand the effect of the intrinsic nature of a particular metal on SR of ethanol activity as well as selectivity.

In fact, the SR of ethanol is composed of a bifunctional mechanism. Dehydrogenation and dehydration reactions take place mainly on the support, and the dehydrogenation reactions are promoted at the metal and metal–support interface.⁴⁵ However, decomposition reactions occur on the surface of the metal particles.

2.1.3. Reaction Mechanism in Aqueous-Phase Reforming and Reforming in Supercritical Water. Hydrogen can also be produced by aqueous-phase reforming (APR) of oxygenated compounds derived from biomass such as ethanol.⁴⁹ Compared to the SR of ethanol in the vapor phase, the APR of ethanol eliminates the need to vaporize both water and ethanol. Therefore, the energy-intensive distillation of ethanol/water mixtures is no longer required, reducing the costs of the process. In addition, APR is carried out at lower temperatures than SR; this minimizes undesirable decomposition reactions. Furthermore, hydrogen is produced with

low levels of CO because the WGS reaction is favored at APR process temperatures. However, the APR of the ethanol process is composed of several steps. When sugar cane is the source, ethanol is first obtained by carbohydrate fermentation and distillation. This is followed by hydrogen production via APR of the ethanol. However, hydrogen can also be directly produced from carbohydrates by APR, foregoing the need to first generate ethanol.

Basically, the same reactions observed for SR of ethanol also occur during APR. Cruz et al.⁵⁰ studied APR of ethanol over Ni obtained from hydrotalcite precursors. The best catalyst exhibited an ethanol conversion of around 70%. H₂, CO₂, CH₄, CO, and acetaldehyde were the products formed in the gas phase. CH₄, CO, and H₂ were produced by ethanol decomposition. In addition, it has been suggested that the low levels of CO formed are due to the WGS reaction. This reaction is thermodynamically favored at lower reaction temperatures. The same products were observed during the ethanol APR reaction over a Pt/Al₂O₃ catalyst.⁵¹ The formation of alkanes (CH₄, C₂H₆) using the APR process for hydrogen production remains a challenge. It requires the development of an efficient catalyst for promoting C–C bond cleavage that at the same time inhibits scission of the C–O bond.

Catalytic reforming of ethanol in supercritical water (SCW) is also a promising technology for hydrogen production^{52–54} for several reasons: (i) it does not require the evaporation of water; (ii) hydrogen is produced at high pressure and can be stored directly, eliminating the costs associated with compression; and (iii) mass-transfer limitations are reduced due to the high diffusivity of supercritical fluids.

Hydrogen was produced by ethanol reforming in SCW over a Ru/Al₂O₃ catalyst with low levels of methane and CO.⁵² Hydrogen formation was favored at high temperature and high water-to-ethanol molar ratios. On the other hand, pressure did not affect the hydrogen yield. The mechanism proposed for ethanol reforming in SCW was similar to that reported for SR of ethanol below the critical pressure of water (22.1 MPa). It involves ethanol dehydrogenation to acetaldehyde, followed by decomposition to CO and CH₄ as well as the WGS reaction, which produces CO₂ and H₂. The reaction of CO with water is fast, and hence, only traces of CO are detected in the gas phase. Using a Ru/C catalyst, Rabe et al.⁵³ came to the same conclusion that the mechanism of ethanol reforming under SCW proceeds by the same reaction pathways described for the SR of ethanol at low pressure.

2.2. Spectroscopic and Thermal Desorption Studies

2.2.1. Fundamental Mechanistic Studies on Transition Metal Surfaces.

The early fundamental mechanistic studies focused on the decomposition pathways of oxygenated compounds on single-crystal transition metal surfaces.^{55–60} The spectroscopic identification of surface reaction intermediates was accomplished by using ultra-high vacuum (UHV) surface science techniques such as low-energy electron diffraction (LEED), high-resolution electron energy loss spectroscopy (HREELS), Auger electron spectroscopy (AES), X-ray photoelectron spectroscopy (XPS), and temperature-programmed desorption mass spectrometry (TPD-MS). Recently, density functional theory (DFT) calculations were also applied in an effort to shed light on the likely reaction pathways operating for ethanol conversion over different metals.^{61–65}

Ethanol reactions on transition metal surfaces are composed of a complex system, which includes several reaction intermediates, such as alkoxides, aldehydes (e.g., η^1 and η^2), acyl species, and carboxylates. Figure 4 shows the main oxygenated species observed for reactions over transition metal surfaces.⁵⁸

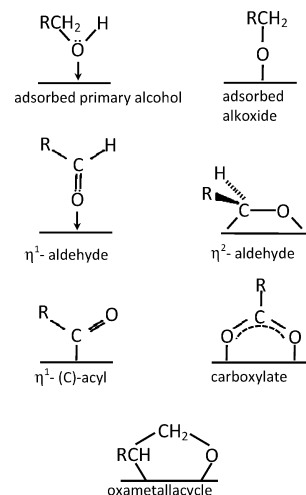


Figure 4. Main oxygenate intermediates adsorbed on transition metal surfaces. Reprinted with permission from ref 58. Copyright 1998 Elsevier.

Mavrikakis and Bartea⁵⁸ reviewed the decomposition mechanisms of alcohols and aldehydes on transition metal surfaces (i.e., from groups VIII and IB). A typical reaction pathway for ethanol decomposition (ED) on palladium and rhodium surfaces is shown in Figure 5. The first step involves

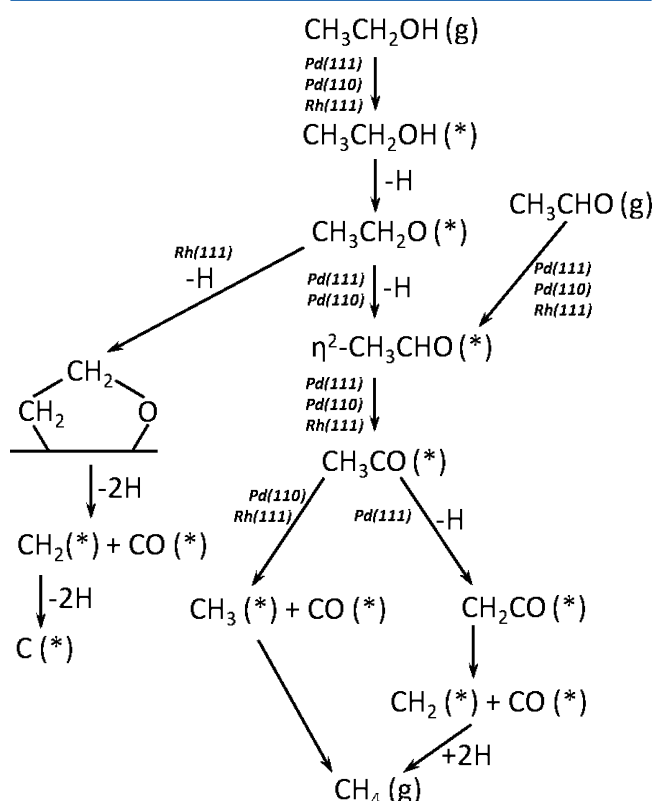


Figure 5. Reaction pathways observed for ethanol adsorption over transition metal surfaces. Reprinted with permission from ref 58. Copyright 1998 Elsevier.

the formation of an ethoxy species through the dissociative adsorption of ethanol. This involves the donation of a lone pair of electrons from oxygen to the surface, followed by O–H bond cleavage. Scission of the C–O bond does not occur,

although the energy of the O–H bond is higher than that of the C–O bond in the gas phase.^{66,67} DFT calculations resulted in an activation energy of 51 kJ/mol for O–H bond cleavage and ethoxy formation (Figure 6).⁶¹ The second step consists of

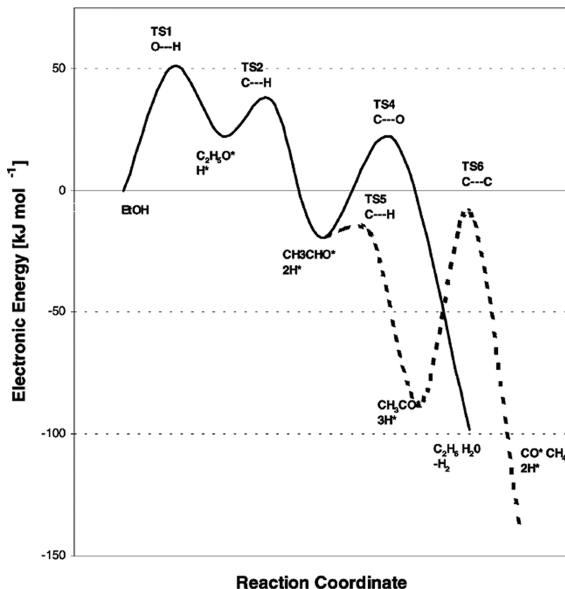
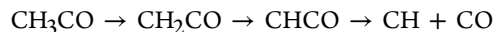


Figure 6. Reaction energy diagram for ethanol reactions on Pt(111) from the DFT study. Reprinted with permission from ref 61. Copyright 2001 Elsevier.

eliminating an α -hydrogen from the ethoxy intermediate. This produces an aldehyde intermediate that may be bonded to the metal surface either through the oxygen atom ($\eta^1(O)$ configuration) or via the oxygen and carbon atoms of the carbonyl group ($\eta^2(C,O)$ configuration).⁵⁸ Carbonyl compounds bonded to the metal surface through the $\eta^1(O)$ configuration are less stable and tend to desorb more readily. The adsorption configuration also depends on the nature of the metal. For group VIII metal surfaces, both geometries can exist; the $\eta^1(O)$ configuration is preferred for group IB metal surfaces.⁵⁸ According to DFT calculations, the activation energy barrier of this step is low (15 kJ/mol).⁶¹ Adsorbed acetaldehyde species can react by means of three different reaction pathways, each resulting in different products: (i) desorption of acetaldehyde to produce gaseous acetaldehyde; (ii) cleavage of the C–O bond of acetaldehyde and addition of hydrogen to form ethane and water; or (iii) acetyl species formation, which requires additional hydrogen removal from acetaldehyde.⁶¹ DFT calculations indicated that C–H bond scission with concomitant formation of acetyl species is the energetically favored route. It has an activation energy of only 1 kJ/mol, whereas C–O bond scission exhibits a higher activation energy of 39 kJ/mol (Figure 6).⁶¹ Moreover, the formation of an acetyl intermediate over different metal surfaces has been experimentally confirmed by HREELS.^{56,68} The acetyl species can undergo further decomposition through C–C bond cleavage to produce adsorbed CH_3 and CO species.^{60,69} Hydrogenation of the CH_3 species thus formed results in the evolution of methane. This CH_3 species can also be further dehydrogenated to form CH_x species (CH_2 and CH) and C. However, the calculated activation energy corresponding to direct cleavage of the C–C bond of adsorbed CH_3CO is 117 kJ/mol, compared to 79 kJ/mol for C–C bond scission of CHCO species.⁶¹

Therefore, it was proposed that C–C bond scission proceeds sequentially through the following series of steps:



DFT calculations were used to study the nature and stability of the surface intermediates formed in the ethanol hydrogenolysis reaction over various transition metals (e.g., Cu, Pt, Pd, Ni, Ir, Rh, Co, Os, Ru, Re). The potential energy surface for C–C and C–O bond breaking in ethanol for all 24 possible intermediates formed on the transition metals under study was determined.⁶² The results predict that cleavage of the C–C bond of the $\text{CH}-\text{CO}$ intermediate is the rate-determining step.

This reaction scheme has been proposed to operate for ED on Pd, Pt, Ni, Ru, and Rh surfaces. However, another reaction pathway has been reported in the literature for Rh(111) surfaces.⁵⁸ In this case, it is suggested that ED proceeds by the abstraction of a β -hydrogen, leading to the formation of an oxametallacycle, which undergoes direct decomposition to methane and CO, foregoing the acetaldehyde formation step.

There are also variations of the previously described ED reaction mechanisms over metal surfaces.^{55,60,69} For instance, the decomposition of ethanol could take place by direct decomposition of the ethoxy species to give methane, hydrogen, and CO, thereby dispensing with the steps involving the formation and decomposition of acetaldehyde and acetyl intermediates. In the case of ethanol adsorption over an oxygen-precovered surface, the formation of acetate can also occur.⁶⁹ This acetate species can decompose to produce H_2 , CO_x , and CH_x species.

2.2.2. Oxygenate Reaction Pathways on Oxides and Supported Metal Catalysts. Several spectroscopic investigations regarding ethanol and acetaldehyde reactions over oxides and supported catalysts have been reported in the open literature.^{29,31,66,70–84} Although basically the same intermediates have been observed on transition metal surfaces as identified over either metal oxides or metal oxide-supported metal catalysts, there are remarkable differences among these systems. The oxidation products, resulting from ethanol transformation (e.g., acetate, carbonate), are present to a greater extent in the spectra of ethanol adsorbed over metal oxides and metal oxide-supported metals because of the availability of oxygen on the surfaces of these materials. Acetate species are detected even at room temperature on unreduced CeO_2 surfaces⁷¹ as well as on Pt/CeO_2 ,⁸² Pd/CeO_2 , and Co/CeO_2 ⁸³ catalysts.

Tables 1 and 2 list the infrared vibrational wavenumbers and mode assignments for the different adsorbed species that have been observed during infrared experiments on metal oxides and supported metal catalysts.^{31,37,66,70,71,75–77,84–86} It is important to note that there are some discrepancies in the mode assignments of some bands among the literature data. A general scheme presenting all the reaction pathways of ethanol over oxides and supported metal catalysts is shown in Figure 7.

Ethanol adsorbs dissociatively over the metal oxide cation ($\text{Me} = \text{Ce}^{4+}, \text{Al}^{3+}, \text{Ti}^{4+}$) as an ethoxy species in either a monodentate or bidentate mode. For instance, ethoxy species are adsorbed over a single Ce^{4+} cation in a monodentate mode on the $\text{CeO}_2(111)$ surface. On the other hand, ethoxy species in a bidentate mode are formed over two step-flat Ce^{4+} cations on $\text{CeO}_2(310)$.⁶⁶ The ethoxy bands are shifted to lower wavenumbers when the ethoxy species are adsorbed onto a Me cation close to an oxygen vacancy (e.g., associated with reduced Ce^{3+} centers) or a metal cluster.⁶⁶ Ethanol can also be molecularly

Table 1. Infrared Vibrational Wavenumbers and Mode Assignments for the Adsorption of Ethanol on Different Catalysts

vibrational mode	adsorbed species	ethanol								
		CeO ₂ ^a	Pd/CeO ₂ ^a	Pt/CeO ₂ ^b	Pt/CeO ₂ ^c	Pt/TiO ₂ ^c	Pt/Al ₂ O ₃ ^d	Ir/Al ₂ O ₃ ^e	Pt/CeZrO ₂ ^f	Pt/CeZrO ₂ ^g
ν_{as} (CH ₃)	ethoxy/acetate	2960	2983	2978	2981	2969	2974	2973	2977	2978
ν_{as} (CH ₂)	ethoxy		2934	2933		2928	2930	2931	2935	2935
ν_s (CH ₂)	ethoxy	2832	2909	2909	2896		2902	2903	2906	2898
ν_s (CH ₃)	ethoxy/acetate		2880	2878	2872	2870	2877	2875	2880	
δ (CH ₂)	ethoxy	1473	1477	1478					1473	
δ_{as} (CH ₃)	ethoxy		1453	1451	1445	1445	1450	1448	1452	1452
δ_s (CH ₃)	ethoxy	1383	1397	1399	1391	1398	1392	1390		1408
δ (OH)	molecular ethanol		1266	1264	1264	1267	1276	1277		
ρ (CH ₃)	ethoxy					1135	1161	1166		
ν (CO)mono	ethoxy	1107			1100		1106	1118		
ν (CO) mono	ethoxy		1086	1082	1072	1076	1073	1095	1081	1081
ν (CO) bi	ethoxy	1057	1039	1038	1042	1040	1052	1052	1045	1045
ν_{as} (OCO)	acetate	1580				1550	1570	1560	1545	1550
δ_{as} (CH ₃)	acetate	1437								
ν_s (OCO)	acetate	1426				1460	1472	1478	1425	1425
δ_s (CH ₃)	acetate	1304							1350	1342
ν_{as} (OCO)	carbonate	1568	1527	1530					1538	
ν_s (OCO)	carbonate	1428	1442	1423					1431	
ν_s (OCO)	carbonate	1341	1349	1353						
ν (CO)	acetaldehyde		1704	1692			1693		1703	
ν (CO)	crotonaldehyde		1659		1647	1635				
ν (C=C)	crotonaldehyde		1637		1613					
ν (CO)	acetyl								1627	
ν (CO)	adsorbed CO (bridged)					1970			1938	
ν (CO)	adsorbed CO (linear)				2012	2030	2017	2019	2033	2027

^aReference 71. ^bReference 66. ^cReference 77. ^dReference 31. ^eReference 76. ^fReference 37. ^gReference 37 under SR reaction mixture.

Table 2. Infrared Vibrational Wavenumbers and Mode Assignments for the Adsorption of Acetaldehyde, Acetone and Acetic Acid on Different Catalysts

vibrational mode	adsorbed species	acetaldehyde				acetone		acetic acid		
		CeO ₂ ^a	Pd/CeO ₂ ^a	Pt/Al ₂ O ₃ ^b	Pt/CeO ₂ ^c	TiO ₂ ^d	Pt/ZrO ₂ ^e	CeO ₂ ^f	Pd/CeO ₂ ^a	Pt/CeZrO ₂ ^g
ν_{as} (CH ₃)	ethoxy/acetaldehyde/acetone	2965	2979	2963		2973				
ν_{as} (CH ₂)	acetate	2930								
ν_s (CH ₃)	ethoxy/acetaldehyde/acetone	2870		2923		2931				
δ_{as} (CH ₃)	ethoxy	1376								
ρ (CH ₃)	ethoxy		1114							
ν (CO)	ethoxy/acetate	1067							1053	
ν (CO)	acetate						1026	1020	1024	
ν_{as} (OCO)	acetate	1559	1550	1564	1545	1543	1580	1568	1552	
δ_{as} (CH ₃)	acetate							1451	1454	
ν_s (OCO)	acetate	1423	1450		1413	1436	1429	1400	1415	
δ_s (CH ₃)	acetate	1334	1343		1353		1306	1340	1340	
ν (OCO)	carbonate			1478						
ν (OCO)	carbonate			1350						
δ_{as} (CH ₃)	acetaldehyde			1451						
δ_s (CH ₃)	acetaldehyde			1391						
ν (CO)	acetaldehyde		1715	1692	1720				1699	
ν (CO)	crotonaldehyde	1662		1635						
ν (C=C)	crotonaldehyde	1600		1609						
ν (CO)	acetyl		1685		1669					
ν (CO)	acetone				1702					
δ_{as} (CH ₃)	acetone				1422					
δ_s (CH ₃)	acetone				1366	1402				
ν_{as} (C-C)	acetone				1240					
ν (CO)	adsorbed CO (bridged)		1929							
ν (CO)	adsorbed CO (linear)		2070							

^aReference 70. ^bReference 75. ^cReference 84. ^dReference 85. ^eReference 86. ^fReference 71. ^gUnpublished results.

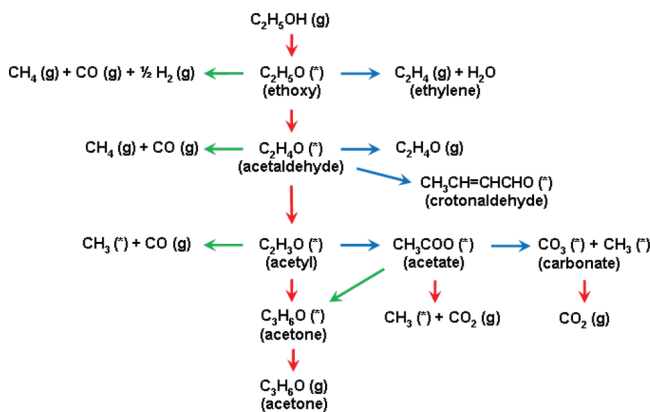


Figure 7. Reaction pathways of ethanol over supported metal oxides.

adsorbed onto Lewis acid sites of metal oxides. Domok et al.³¹ attributed the band at around 1270 cm^{-1} to the $\delta(\text{OH})$ mode of ethanol coordinatively bonded to Al^{3+} . This molecularly adsorbed ethanol is postulated as being responsible for the ethanol desorption peak at low temperatures in the temperature-programmed desorption (TPD) profile.

The ethoxy species can be further dehydrogenated to form acetaldehyde, and this process is facilitated by the presence of either hydroxyl groups (e.g., SR, OSR) or oxygen (e.g., POX, OSR) on the catalyst surface. The conversion of acetaldehyde can follow a number of different reaction pathways:

- (i) Acetaldehyde can desorb to produce acetaldehyde in the gas phase;
- (ii) Acetyl species can be formed from the acetaldehyde by the abstraction of additional hydrogen. The identification of this band is controversial and merits further comments. Acetyl species on metal surfaces exhibit a $\nu(\text{CO})$ mode between 1610 and 1670 cm^{-1} .⁵⁶ As a comparison to these studies with those of metal oxides, bands in this region of the IR spectra have been attributed to acetyl species. However, bands in this region have also been assigned to crotonaldehyde or even to the bending mode of water. The pair of bands at around 1660 and 1630 cm^{-1} has been ascribed to the $\nu(\text{C=O})$ and $\nu(\text{C=C})$ modes of adsorbed crotonaldehyde, formed by the β -aldolization of two acetaldehyde molecules;^{66,70–73}
- (iii) Acetaldehyde can also be oxidized to acetate species by hydroxyl groups from the support.³¹

In addition, acetate species can also be formed by the reaction between the acetyl species and oxygen from the support. Acetate species have been extensively reported in the literature as important intermediates during ethanol conversion reactions, and their decomposition pathways dictate not only the selectivity but also the stability of the catalysts.^{37–39,70,71,76,77,80,82,83} Erdőhelyi et al.⁷⁶ observed that variations in the integrated absorbances of the acetate species were the same, regardless of the nature of the metal (Pt, Pd, Ir, Rh, Ru) supported over Al_2O_3 . This indicates that the formation of acetate species takes place on the metal oxide. The acetate species can either decompose to form CH_4 and CO or further oxidize to produce carbonate species.

According to the assignments of the vibrational modes for acetate and carbonate species, it is difficult to distinguish one species from another by examining vibrational modes in the $\nu(\text{OCO})$ stretching region. However, the disappearance of

bands in the C–H stretching region can be monitored in conjunction with those in the $\nu(\text{OCO})$ stretching region in order to follow the conversion of acetate to carbonate species.

TPD of adsorbed ethanol and monitoring of the gas-phase composition during infrared experiments^{37,39,66,71,72,82–84,87–89} have revealed that dehydrogenated species (e.g., ethoxy, acetaldehyde, and acetyl species) can undergo decomposition to form CO, CH_4 , and H_2 at relatively low temperatures. Yee et al.^{66,71} observed the formation of CO, CH_4 , and CO_2 during the TPD of ethanol on CeO_2 and Pd/CeO_2 . However, these products were formed at high temperature (730 K) on a CeO_2 sample. This result confirms that the decomposition of dehydrogenated species takes place either on the metal particles or with the assistance of the metal particle at the metal–support boundary.

Acetone, ethylene and benzene formation have also been detected in some TPD experiments during ethanol desorption.^{66,71,72,81,87–89} There are two possible routes that can be used to explain acetone formation. The first involves the coupling of two acetate molecules, and the second is the disproportionation of two acetyl species.⁷¹ The IR vibrational modes that are characteristic of acetone and acetaldehyde are very close, and thus, a clear identification of these compounds by using only IR spectroscopic results is at the very least difficult, and possibly even unfeasible (Table 2).

Ethanol dehydration to ethylene can occur by one of two different mechanisms depending on the acid/base properties of the support.⁹⁰ Acidic supports such as alumina promote the dehydration of ethanol to ethylene via an E_2 mechanism, which requires strong Lewis acid sites and basic sites. The E_{1cB} mechanism involving both strongly basic sites and weak Lewis acid sites is characteristic of basic materials. The dehydration of ethanol to ethylene over different zeolites and silica–alumina revealed that ethylene is produced via a two-step dehydration.⁹¹ The first step involves the formation of diethyl ether as a result of intermolecular dehydration from two ethanol molecules. This is followed by a second dehydration of diethyl ether to ethylene. The dehydration activity was correlated to the number of strong Brønsted acid sites on the catalysts. The direct conversion of ethanol to ethylene can occur at high reaction temperatures.⁹² Ethylene can undergo further reactions such as oligomerization, aromatization, or cracking, producing benzene, toluene, or xylenes (BTX). These reactions may be responsible for coke formation and catalyst deactivation. This will be discussed in more depth in section 3.

Coupling reactions of ethanol or acetaldehyde can also occur and depend on specific combinations of acid and base sites on the catalyst surface.⁹³ For example, *n*-butanol can form as a result of the direct condensation of ethanol as well as through acetaldehyde condensation followed by dehydration and hydrogenation steps. To date, most of the ethanol reaction mechanisms proposed in the literature have relied on infrared spectroscopy data measured under vacuum and not under realistic reaction conditions.

For instance, diffuse reflectance infrared Fourier transform spectroscopy (DRIFTS) was used by Song and Ozkan⁸⁰ to monitor the surface species adsorbed on 10% Co/ZrO₂ and 10% Co/CeO₂. First, an ethanol TPD experiment was carried out over Co/ZrO₂ and Co/CeO₂. At room temperature, a negative band appeared at 3600 – 3800 cm^{-1} . This was attributed to the molecular adsorption of ethanol and the formation of hydrogen bridge bonded with the OH groups of the support. Furthermore, the authors attributed the vibrational bands located at 1323 and 1280 cm^{-1} to the $\delta(\text{CH}_3)$ and

$\delta(\text{OH})$ vibrational modes of molecularly adsorbed ethanol. Ethanol adsorption also led to dissociatively adsorbed monodentate and bidentate ethoxy species, as defined by bands characteristic of CH_3 bending ($1443, 1381 \text{ cm}^{-1}$) and $\nu(\text{CCO})$ stretching ($1161, 1110, 1066 \text{ cm}^{-1}$) modes, as well as bands corresponding to the $\nu(\text{C}-\text{H})$ stretching modes of CH_3 and CH_3-CH_2 groups. The latter are positioned between 3000 and 2700 cm^{-1} , with major bands located at $2970, 2928, 2867$, and 2710 cm^{-1} . With increasing temperature, the bands characteristic of the ethoxy species disappeared. It was suggested that this could be due to their oxidation to surface acetate species by support-bound oxygen. This assignment was made based on the formation of bands at 1552 cm^{-1} of $\nu_{\text{as}}(\text{OCO})$, 1441 cm^{-1} of $\nu_s(\text{OCO})$, and 1346 cm^{-1} for $\delta(\text{CH}_3)$. It was then suggested that the acetate species reacted to form monodentate carbonate as an intermediate, which in turn dissociated to give CO_2 , as evidenced by the gas-phase band. Interestingly, over the CeO_2 -supported catalyst, the catalytic cycle occurred at much lower temperatures. Even at room temperature, the vibrational bands of acetate species were present. The authors suggested that this was due to an abundance of surface oxygen available for reaction with the ethoxy species. No species remained on the surface at $400 \text{ }^\circ\text{C}$, whereas acetate bands were still evident at $500 \text{ }^\circ\text{C}$ over the Co/ZrO_2 catalyst. DRIFTS spectra were also obtained after adsorption of both ethanol and water at room temperature followed by heating under helium for both Co/ZrO_2 and $\text{Co}/\text{CeO}_2-\text{ZrO}_2$ catalysts. Similar features were observed during the TPD of ethanol, although additional bands characteristic of H_2O were also present. However, steam addition appears to facilitate ethanol conversion, since the bands characteristic of surface acetate species disappeared at lower temperatures. With the CeO_2 -containing catalyst, the acetate species disappeared at even lower temperatures than that observed for Co/ZrO_2 ; again, the authors attributed this finding to the increased accessibility of intermediates to support-bound oxygen.

Alternatively, TPD of adsorbed ethanol has also been employed extensively to study the adsorption properties of ethanol for different catalytic systems such as $\text{Ni}/\text{Al}_2\text{O}_3$,¹⁵ $\text{Pt}/\text{Al}_2\text{O}_3$,⁷⁸ $\text{Pd}/\text{Al}_2\text{O}_3$,^{87–89} Ir/CeO_2 ,³⁶ Pd/CeO_2 ,⁷¹ Pt/CeO_2 ,^{66,82} Rh/CeO_2 ,⁷² Co/CeO_2 ,⁸⁰ Co/ZrO_2 ,⁸⁰ Co/ZnO ,⁹⁴ and $\text{Ni}/\text{La}_2\text{O}_3$.¹⁵

TPD profiles of adsorbed ethanol on $\text{Pd}/\text{Al}_2\text{O}_3$ ^{87–89} reveal three distinct features. In the low-temperature region (below 700 K) occur (i) the dehydration of ethanol to ethylene; (ii) the dehydrogenation of ethanol to acetaldehyde; and (iii) the decomposition of ethanol to CO , CH_4 , and H_2 . Cordi and Falconer⁸⁸ suggested that part of the ethanol adsorbed on alumina forms an ethoxy species that migrates to Pd sites, where decomposition takes place. The α -carbon produced CO and the β -carbon formed CH_4 during ethanol decomposition. The detection of CO , CO_2 , and H_2 at high temperatures was attributed to the decomposition of a more stable carbon species formed previously when the ethanol decomposed at the lower temperatures. de Mello et al.⁸⁹ suggested that, while ethanol (adsorbed as ethoxy species) is dehydrogenated on Pd sites to form acetaldehyde, more stable acetate species are also formed as revealed by IR spectra. These species remain adsorbed and are the precursors for CO , CO_2 , and H_2 production at high temperature.

Additional products are observed in the TPD profile of adsorbed ethanol on ceria-supported catalysts such as acetone,

crotonaldehyde, and butene.^{66,71,72,82} These are products of ethanol or acetaldehyde condensation reactions.

2.2.3. Obtaining Mechanistic Information under Reaction Conditions. Although the investigations described made important progress toward elucidating the mechanisms of ethanol conversion, the main drawback is that they were not carried out under reaction conditions, which would involve flowing the reaction mixture at different temperatures. However, the nature of the intermediate species formed on the surface may be strongly affected by the reaction conditions.³⁷ Recently, infrared spectroscopy data has been used to postulate mechanisms based on changes observed in the concentrations of surface species under ethanol reforming reaction conditions that more closely mimic a realistic feed.

Llorca et al.⁹⁴ conducted the SR of ethanol over 10 wt \% Co/ZnO and ZnO catalysts. The authors proposed that, if the dehydrogenation of ethanol to acetaldehyde is the first step, then the reforming of acetaldehyde should be favored over Co/ZnO relative to ZnO . To test this hypothesis, DRIFTS was performed while the ethanol SR reaction was carried out over both catalysts in the temperature range of 200 – $300 \text{ }^\circ\text{C}$. Simultaneously, the products H_2 , CO_2 , CH_4 , acetaldehyde, and dimethyl ketone were detected by mass spectrometry. From the DRIFTS spectra in the 200 – $300 \text{ }^\circ\text{C}$ range, ethoxy species ($\text{mono-}\nu(\text{CO}) = 1096 \text{ cm}^{-1}$; $\text{bidentate-}\nu(\text{CO}) = 1055 \text{ cm}^{-1}$) were observed over Co/ZnO , while for ZnO , bidentate ethoxy species ($\nu(\text{CO}) = 1050 \text{ cm}^{-1}$) were the main bands reported. Weak bands in the range 1600 – 1400 cm^{-1} were also obtained. A band at 1713 cm^{-1} for Co/ZnO was tentatively assigned to physisorbed acetaldehyde. By raising the temperature to $400 \text{ }^\circ\text{C}$ and quenching in helium, a number of bands of interest were observed. For Co/ZnO , the $\nu(\text{C}-\text{O})$ bands of mono- and bidentate ethoxy species, as well as a series of bands between 1700 and 1300 cm^{-1} (e.g., $1660, 1591, 1555, 1450, 1380$ and 1343 cm^{-1}), were evident. A number of these bands were assigned to surface acetate species ($\nu_{\text{as}}(\text{OCO}) = 1591, 1555 \text{ cm}^{-1}$; $\nu_s(\text{OCO}) = 1450$ and 1380 cm^{-1} ; and $\delta(\text{CH}_3) = 1343 \text{ cm}^{-1}$). On the basis of the separation between the asymmetric and symmetric bands, the authors suggested that these species exhibited the bidentate or bridge conformation. The 1660 cm^{-1} band was attributed to acetyl species. In the case of ZnO , broad bands with maxima at 1574 and 1453 cm^{-1} were observed and assigned to similar bidentate or bridged surface acetate species. Carrying out the TPD experiment after quenching with inert gas, hydrogen, carbon dioxide, acetaldehyde, methane, dimethyl ketone, and ethanol were detected by mass spectrometry. In addition, the intensity of the bands related to ethoxy species decreased in the DRIFTS experiment. One possibility is that ethoxy species can convert to acetaldehyde through H-elimination over ZnO . Then, the aldehyde can undergo nucleophilic attack by lattice oxygen at the carbonyl carbon of the aldehyde. This in turn can be followed by either hydride elimination to produce surface carboxylate (which can further undergo decomposition to CO_2 , carbon, and H_2O at higher temperatures) or alkyl elimination to produce formate and stable surface alkyl species at low temperatures.

Lin et al.⁹⁵ studied the effect of the crystalline structure of metallic cobalt [unsupported Co (hexagonal close-packed (hcp), face-centered cubic (fcc))] on the SR of ethanol using DRIFTS experiments carried out under actual reaction conditions. For the more active hcp Co catalyst, only bands representative of gas-phase CH_4 , CO_2 , CO , and acetone were identified initially. With time, however, as the catalyst

underwent deactivation, intermediate and reactant bands such as acetaldehyde and ethanol were detected. With the less-active fcc Co catalyst, the intermediates were detected even in the initial stages of the reaction. With 10% ceria addition, the two additional bands observed at 1530 and 1428 cm⁻¹ were assigned to carbonate species on CeO₂. The presence of smaller bands for adsorbed ethanol and carbonyl-containing intermediates (e.g., acetone and acetaldehyde) and a more intense CO₂ band suggested that ceria promotes the C–C bond breaking of ethanol and intermediate species to form CO₂ and H₂.

Both the activation and turnover of different molecules on 1 wt %Pt/cevia were followed by Jacobs et al.⁹⁶ Activation of the catalyst leads to the formation of type II bridging OH groups;⁹⁶ these are hydroxyl groups associated with Ce³⁺ defect sites, which can be formed in one of two ways. If hydrogen is used, it will first reduce the noble metal and then dissociate on the surface; the dissociated hydrogen will spill over to the support and form the OH groups directly (Figure 8). Because O

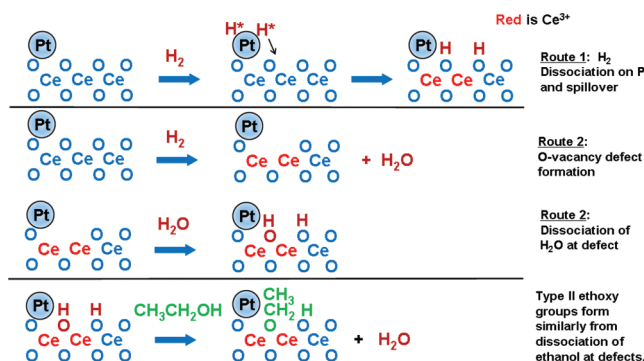


Figure 8. Scheme of activation of ethanol by type II ethoxy group formation. Reprinted with permission from ref 37. Copyright 2008 Elsevier.

adatom is converted to –OH, the associated Ce⁴⁺ atoms are reduced to Ce³⁺. The second manner in which they can be formed is through oxygen vacancies.⁹⁶ In this interpretation, H₂ reacts with O adatoms to generate O-vacancies and H₂O. Once again, the cerium atoms associated with the defect—in this case, an oxygen vacancy—are converted to the Ce³⁺ oxidation state. Then, H₂O will dissociate at the defect to generate the type II bridging OH groups indirectly. Type II refers to the greater interaction of the adsorbed species with the support relative to type I species, due to the fact that a defect site is present (i.e., Ce is reduced to the Ce³⁺ oxidation state). This is why type II species appear at lower wavenumbers relative to type I species. Ethanol is activated on the surface in the same manner as H₂O. Ethanol was observed to adsorb in a dissociative manner to form defect-associated bridging ethoxy species (1060–1080 cm⁻¹). These are also type II species from infrared investigations. Steaming led to a decrease in the ethoxy bands and an increase in the acetate bands ($\nu_{as}(\text{OCO})$ 1540–1560, $\nu_s(\text{OCO})$ 1340, $\nu(\text{CH})$ 2930, 2850–2875 cm⁻¹). This indicates that the ethoxy species underwent oxidative dehydrogenation. Continuing steaming, it was shown that the acetate bands demethanated to form carbonate species ($\nu(\text{OCO})$ at 1290, 1345–1350, 1460, 1500, and 1565 cm⁻¹), and only at that point the gas-phase CO₂ band was observed. Analogies were also developed among SR, WGS, and methanol steam reforming reactions. For example, the oxidative dehydrogenation of ethoxy species to acetate was

linked to the oxidative dehydrogenation of methoxy species to formate as previously observed in methanol steam reforming investigations. In addition, the steam-assisted forward demethanation reaction was postulated to be analogous to the steam-assisted forward formate decomposition reaction observed in infrared studies of Pt/cevia for both WGS and methanol steam reforming. Although partially reduced ceria was involved in bonding with the oxygen-containing intermediates (e.g., ethoxy, acetate, carbonate), the role of Pt was proposed to assist in the hydrogen transfer reactions by operating across the metal–oxide interface.

A more detailed analysis of the synergy between partially reducible oxide (in this case, ceria-zirconia mixed oxide) and metal (in this case, 1.5 wt % Pt) was carried out by de Lima et al.³⁷ ED, SR, and POX reactions were examined. DRIFTS was used to investigate the reaction mechanisms under reaction conditions. At low temperatures, ethanol was again found to dissociatively adsorb to generate ethoxy species and adsorbed H (as a bridging –OH group). This was confirmed by the formation of ethoxy bands at 1045, 1081, 1407, 1452, 1473, 2880, 2906, 2935, and 2977 cm⁻¹ (Figure 8). At higher temperatures, depending on conditions and reactants used, the catalytic decomposition of the ethoxy species can follow different pathways: (i) decomposition to CO, CH₄, and H₂ or (ii) dehydrogenation to acetaldehyde ($\nu(\text{CO})$, 1703 cm⁻¹) and acetyl species. The dehydrogenated species can in turn undergo support-induced oxidation to give acetate species (1342, 1425, and 1550 cm⁻¹), with either surface O (Figure 9) or –OH

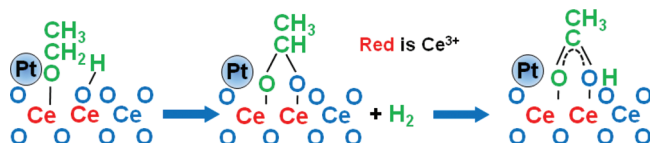


Figure 9. Scheme of transformation of ethoxy to acetate species by surface O. Reprinted with permission from ref 37. Copyright 2008 Elsevier.

(Figure 10) supplying the O required. Thus, Figure 9 may be favored when O₂ is included in the feed, whereas Figure 10 could be preferred when H₂O or another source of –OH is present. Steam also promoted the forward decomposition of acetate to form methane and carbonate as shown in Figure 11. The decrease, as a function of temperature, in the intensities of the bands characteristic of the acetate species was more significant in the spectra in the presence of water (SR). (Figure 12) illustrates the acetate demethanation step. The rates of formation of acetaldehyde and the oxidation of ethoxy species to acetate species were more significant during POX. Here, the support can supply O directly (e.g., redox). SR of ethanol led to significantly lower initial acetaldehyde selectivities and greater initial hydrogen productivities.

A significant trade-off between activity and stability was observed by de Lima et al.⁹⁷ for the case where the catalyst consisted of Pt and ceria compared to that of ceria alone. Although, as previously described, similar ethoxy and acetate bands were observed, at high temperatures the inability of unpromoted ceria to rapidly turn over acetate through forward decomposition was responsible for the high ethylene selectivities observed (i.e., dehydration product). Nevertheless, unpromoted ceria offered very good stability in long-term tests. On the other hand, in the presence of Pt, hydrogen transfer

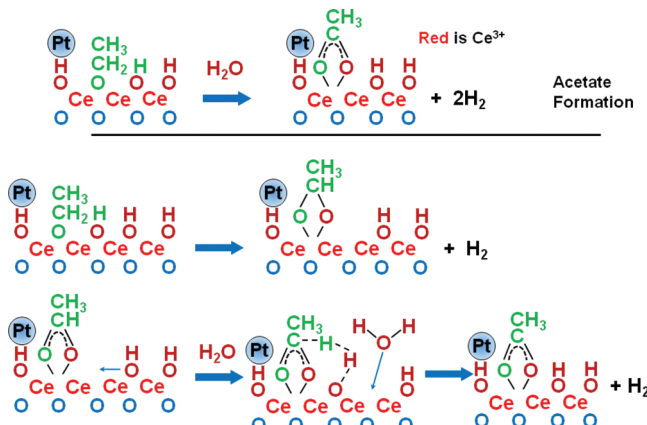


Figure 10. Scheme of transformation of ethoxy to acetate species by surface OH. Reprinted with permission from ref 37. Copyright 2008 Elsevier.

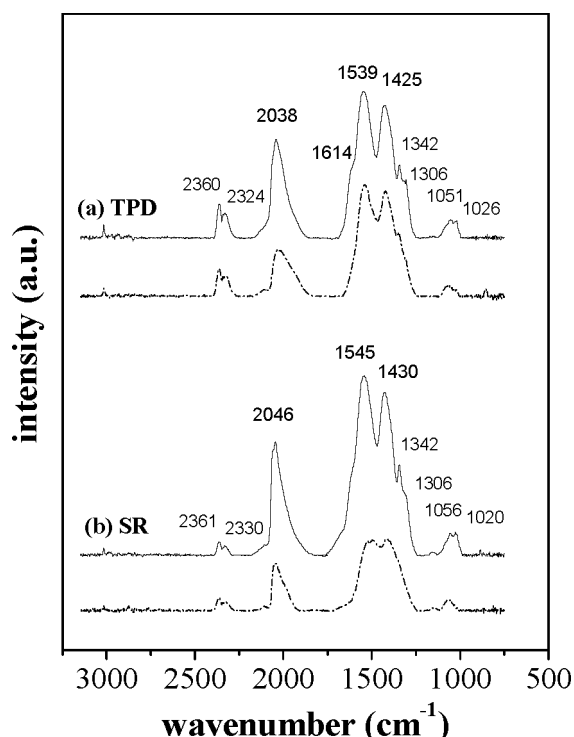


Figure 11. DRIFTS spectra obtained on Pt/CeZrO₂ catalyst at 573 K (solid line) and 673 K (dashed line) and under different reaction conditions: (a) ethanol desorption; (b) SR, the reaction mixture containing ethanol and water (H₂O/ethanol ratio = 2.0). Adapted with permission from ref 37. Copyright 2008 Elsevier.

reactions were facilitated and acetate easily underwent forward decomposition to give CO₂ (via carbonate) and CH₄ (or its surface precursor); the latter presumably underwent further steam reforming. That is, Pt facilitated the H-transfer reaction required to decompose acetate.

A comparison of the DRIFTS spectra for SR obtained over the Pt/ZrO₂, Pt/CeO₂ and Pt/CeZrO₂ catalysts (Figure 13) showed that, in spite of the presence of the same species, significant differences existed in the relative intensities of the bands corresponding to each species. This, in turn, reflects the selectivities of the reaction pathways.⁹⁸ At 313 K, the ratio between the intensities of the acetate species and the ethoxy

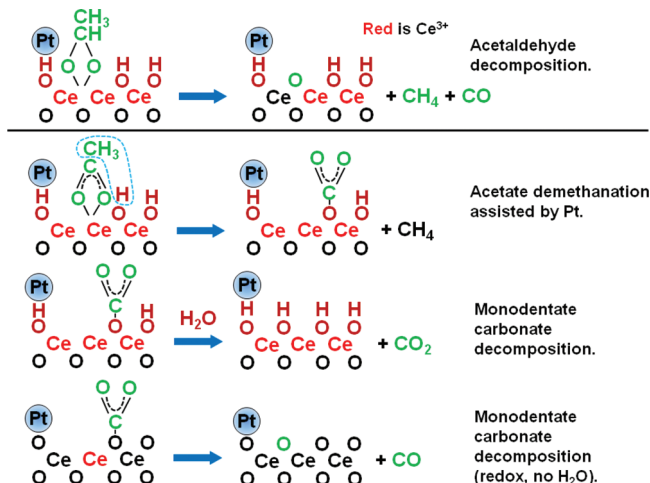


Figure 12. Scheme of acetaldehyde decomposition and acetate demethanation. Reprinted with permission from ref 37. Copyright 2008 Elsevier.

species (acetate/ethoxy ratio) decreased in the order Pt/ZrO₂ > Pt/CeO₂ > Pt/CeZrO₂. This suggests that the transformation of ethoxy to acetate was favored over the Pt/ZrO₂ catalyst (Figure 13a). On the other hand, Pt/CeO₂ exhibited the lowest acetate/adsorbed CO ratio (Pt/ZrO₂ > Pt/CeZrO₂ > Pt/CeO₂) at room temperature. This more than likely reflects a higher Pt dispersion and indicates that the decomposition of ethoxy species to CO, CH₄, and H₂ was facilitated over Pt/CeO₂. At high temperatures, the acetate/adsorbed CO ratio decreased in the order Pt/CeZrO₂ > Pt/ZrO₂ > Pt/CeO₂, indicating that the forward decomposition of acetate was favored over the CeO₂-based catalyst (Figure 13b). In line with the mechanistic arguments derived from DRIFTS data, the highest selectivities to H₂, CH₄, and CO during SR of ethanol at 773 K were obtained for the Pt/CeO₂ catalyst.

Conversion of ethanol with O₂, H₂O, or O₂/H₂O mixture over 10 wt % Co/CeO₂ was examined using DRIFTS³⁸ (Figure 14). Similar findings regarding the mechanism were obtained. At higher temperatures (i.e., 400–500 °C), steam was again found to play a role in promoting the forward decomposition of acetate, whereas the steady-state coverage of acetate was higher for the O₂/H₂O mixture, and highest of all with O₂ alone. DRIFTS spectra for the Rh/Al₂O₃ and Ni–Cu/SiO₂ catalysts recorded under OSR conditions also revealed the presence of acetate species even at relatively high reaction temperatures (400–600 °C).⁹⁹ According to the authors, the conversion of acetate species to carbonate species is most likely the slow step, leading to the accumulation of acetate species on the surface.

2.3. General Overview

On the basis of the papers from the literature, a general reaction mechanism can be postulated for ethanol conversion reactions. Regarding metal oxides and metal oxide-supported metal catalysts, ethanol adsorbs in a dissociative manner to produce ethoxy species. Depending on the acid–base characteristics of the metal oxide, ethoxy species either dehydrate to produce ethylene or dehydrogenate to adsorbed acetaldehyde. Acetaldehyde is a key intermediate of ethanol conversion reactions that can follow different reaction pathways. Acetaldehyde can either desorb or undergo a further hydrogen abstraction, which leads to the formation of acetyl species. Both acetaldehyde and

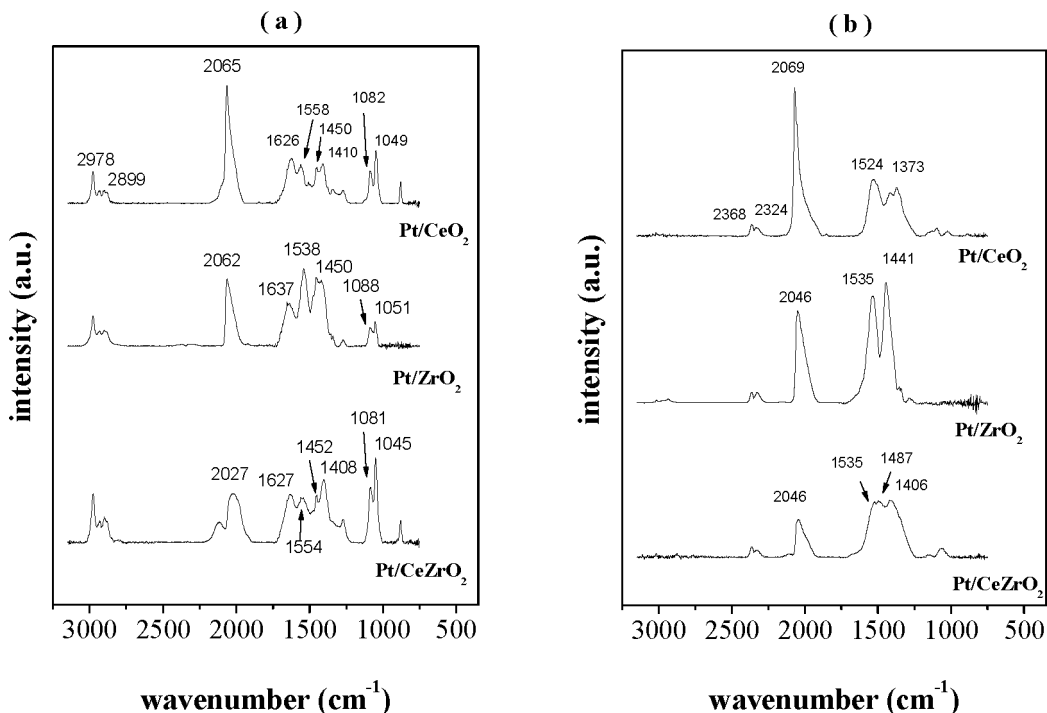


Figure 13. DRIFTS spectra obtained over Pt/CeO_2 , Pt/ZrO_2 , and Pt/CeZrO_2 under the reaction mixture containing ethanol and water (water/ethanol ratio = 2.0) and at (a) 313 K and (b) 773 K. Adapted with permission from ref 98. Copyright 2008 Elsevier.

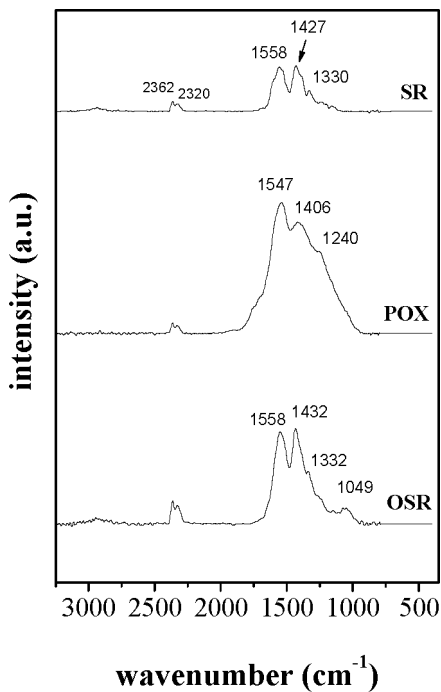


Figure 14. DRIFTS spectra obtained on Co/CeO_2 catalyst at 673 K and under different reaction conditions: (a) SR, the reaction mixture containing ethanol and water ($\text{H}_2\text{O}/\text{ethanol}$ ratio = 2.0); (b) POX, the reaction mixture containing ethanol and oxygen (oxygen/ethanol ratio = 0.5); (c) OSR, the reaction mixture containing ethanol, water, and oxygen ($\text{H}_2\text{O}/\text{ethanol}$ ratio = 2.0; oxygen/ethanol ratio = 0.5). Adapted with permission from ref 38. Copyright 2009 Elsevier.

acetyl species can also be oxidized to acetate species by hydroxyl groups or by oxygen from the support. The acetate species can be further oxidized to carbonate species that decompose to CO_2 . Finally, acetaldehyde can contribute to

the formation of acetone through condensation of acetate or acetyl species. These reactions take place mainly over the support, and the preferred reaction pathway depends on the nature of the metal oxide and the reaction conditions employed. For example, on basic oxides, the rate of ethanol dehydrogenation to acetaldehyde is faster than ethanol dehydration to ethylene. Increasing the reaction temperature or the water/ethanol molar ratio favors the formation of acetate species. The ethoxy species, the dehydrogenated species (acetaldehyde, acetyl species), and the acetate species can all decompose to CO , CH_x , and H_2 . This takes place either at the metal surface or at the metal–support interface. The CH_x species can be hydrogenated and desorb as methane. Alternatively, the CH_x species and CH_4 can react with water, oxygen, and/or CO_2 to produce H_2 and CO . The decomposition reactions occur in the temperature range 573–773 K, whereas the steam reforming, partial oxidation, and dry reforming of methane reactions are favored at higher temperatures (above 773 K). In addition, the nature of the metal directly influences the activity of both the decomposition and steam reforming reactions and, consequently, the production of hydrogen. Where ethanol SR reactions are concerned, Rh is considered to be among the best metals for hydrogen production due to its high activity for C–C bond breaking in ethanol, as well as for its methane steam reforming activity. On the other hand, Pd and Cu exhibit lower activity for C–C bond cleavage, and therefore, they favor acetaldehyde production.

3. CATALYST DEACTIVATION

Catalyst stability is one of the most important challenges in the development of new catalysts for producing hydrogen from ethanol for use in fuel cell applications. Regardless of the metal and support used, significant deactivation during SR has been reported in the literature for applications involving Pt ^{31,39,76}, Pd ,^{23,76} Rh ,^{18,76,100,101} Ru ,^{21,76} Ir ,^{36,76} Co ,^{41,81,102–105} and

Ni-based catalysts.^{14,15,17,106} Catalyst deactivation is generally attributed to the deposition of carbonaceous species as well as either the sintering or oxidation of metallic particles. The main causes of catalyst deactivation are reviewed in the following section.

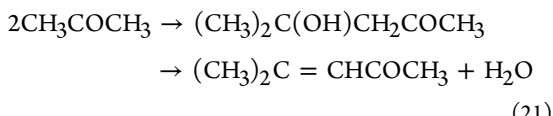
3.1. Carbon Deposition

3.1.1. Reaction Pathways for Carbon Formation. Some of the parallel reactions that take place with ethanol conversion reactions (eqs 1–3) can also lead to catalyst deactivation. The main reactions that contribute to coke formation during ethanol conversion reactions are as follows: (i) ethanol dehydration to ethylene (eq 6), followed by polymerization to coke (eq 20); (ii) aldol condensation of acetone followed by dehydration to mesityl oxide (MO) (eq 21); (iii) the Boudouard reaction (eq 22); (iv) the reverse of carbon gasification (eq 23); and (v) the decomposition of hydrocarbons such as methane (eq 24) and ethylene (eq 25).

- Ethylene polymerization to coke:



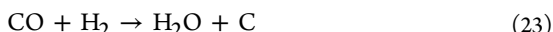
- Acetone conversion to MO:



- Boudouard reaction:



- Reverse of carbon gasification:



- Hydrocarbon decomposition:



The extent of each reaction depends on both reaction conditions and the catalyst used. While low reaction temperatures favor the formation of carbon through reactions 22 and 23, carbon formation via reactions 24 and 25 are the main routes at higher temperatures.^{13,107}

Thermodynamic studies indicate that the region of carbon formation depends on the reaction temperature as well as the water-to-ethanol and oxygen-to-ethanol molar ratios^{7,8,10,12} (Figure 15). The amount of carbon formed during SR of ethanol decreases as the reaction temperature and water-to-ethanol molar ratio increase. For water-to-ethanol molar ratios less than 1, carbon is formed at any temperature. However, carbon is no longer detected for a water-to-ethanol molar ratio of 3 and reaction temperatures above 550 K. For POX of ethanol, the highest mole fraction of hydrogen is observed below an oxygen-to-ethanol molar ratio of 0.5. However, it should be noted that, in this region, significant carbon formation always occurs regardless of reaction temperature.¹² In the case of OSR, an increase in the oxygen-to-ethanol molar ratio reduces the coke-formation boundary region.^{12,13} At 550 K, carbon is not formed for water-to-ethanol molar ratios above 3.0 and oxygen-to-ethanol molar ratios between 0 and 0.9.¹³

There is also experimental evidence regarding the influence of reaction conditions on the degree of carbon formation.^{39,100} The deactivation rate of a 2 wt % Rh/Ce_xZr_{1-x}O₂ catalyst

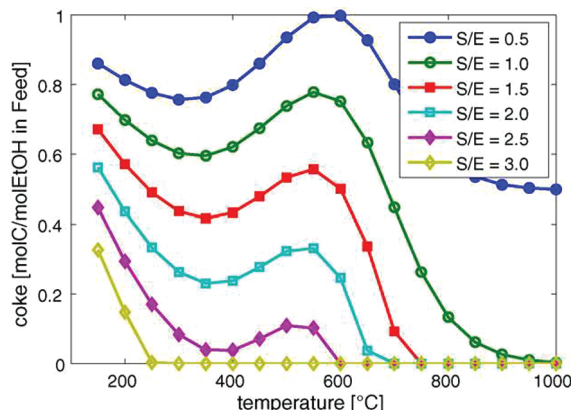


Figure 15. Thermodynamically predicted coke formation for different S/E ratios (mol of H₂O/mol of EtOH) in a fuel processor in steam reforming operation (oxygen-to-ethanol ratio, O/E = 0). Reprinted with permission from ref 12. Copyright 2008 Elsevier.

increased when the SR was carried out at low reaction temperatures and high space velocities, and these conditions contributed to carbon deposition.¹⁰⁰ Significant carbon formation occurred during SR at 773 K over a 1.5 wt % Pt/CeZrO₂ catalyst.³⁹ On the other hand, carbon deposits were not detected when SR was carried out at 1073 K. Increasing space time favored the deposition of filamentous carbon during SR of ethanol over a 10 wt % Co/CeO₂ catalyst.⁴² However, in this case, the amount of carbon formed passed through a maximum and then decreased at higher space times; this trend has been explained in terms of the oxygen mobility of the support. The acid/base properties of the support, which exhibits activity for this reaction,^{3,5} also determine the reaction pathways and, as a consequence, also influence catalyst stability.

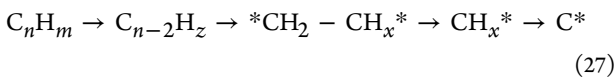
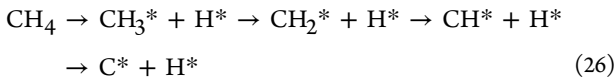
Ethylene formation through ethanol dehydration occurs over acidic (e.g., Al₂O₃) as well as basic (e.g., MgAl₂O₄) supports. However, the selectivity to ethylene over 1 wt % Rh/Al₂O₃ catalyst was 7-fold higher than that of a 1 wt % Rh/MgAl₂O₄ catalyst during SR of ethanol.¹⁰⁸ It should be noted that the polymerization of ethylene to coke takes place on both strong Brønsted and Lewis acid sites of the support.¹⁰⁹ Dehydration and cyclization of alkenes on both strong Brønsted and Lewis acid sites result in the formation of polynuclear hydrocarbons. These remain strongly adsorbed on acid sites and cause loss in activity or form coke multilayers, which results in fouling of the catalyst.¹¹⁰

In addition to polymeric carbon originating from ethylene polymerization, a second source of carbon deposits stems from acetone. The aldol condensation of acetone produces diacetone alcohol, which can then undergo dehydration to mesityl oxide (MO).^{111,112} According to Takanabe et al.,⁸⁶ oligomerization of MO can lead to the formation of coke, resulting in catalyst deactivation.

Furthermore, another type of coke is found that corresponds to CH_x species formed through (i) the decomposition of hydrocarbons (e.g., methane, ethylene) or (ii) the decomposition of dehydrogenated (e.g., ethoxy species and acetaldehyde) and acetate species.

Hydrocarbon steam reforming proceeds by the dissociative adsorption of hydrocarbons on the catalyst surface and involves the direct breaking of C–H bonds; this in turn produces CH_x species that subsequently can generate irreversibly adsorbed carbon (eqs 26 and 27).^{107,113–115} Higher hydrocarbons adsorb

dissociatively much faster than methane, and consequently, coking is more pronounced.¹¹³ Recently, the decomposition of ethylene for the production of CO_x-free H₂ for fuel cells and of carbon nanotubes has been studied.^{116–118}



The decomposition of either ethanol (eq 4) or the acetaldehyde intermediate (eq 8) can also lead to carbon deposition as a result of the decomposition of the methane formed. A DRIFTS study carried out under SR of ethanol reaction conditions demonstrated that there is an accumulation of CH_x species due to an unbalance between the rate of decomposition of dehydrogenated and acetate species to H₂, CO, and CH_x species and the rate of desorption of the CH_x species as CH₄.³⁹ This CH_x species can further decompose to H and carbon, which in turn can result in catalyst deactivation. This depends on the reforming activity of the metal at the reaction temperature.

Decomposition of hydrocarbons and dehydrogenated species, as well as the steam reforming of hydrocarbons, all take place on the metallic sites. Therefore, the nature of the metal site is directly correlated to its activity for these reactions. DFT calculations and Brønsted–Evans–Polanyi correlations were used for modeling ED on 10 transition metal surfaces (i.e., Cu, Pt, Pd, Ni, Ir, Rh, Co, Os, Ru, and Re) and compared with experimental results.⁶² The model-predicted turnover frequencies for C–C bond breaking of ethanol followed the order Rh > Ru > Pt > Ir > Pd > Cu. However, for the relative activities of the metals tested for the methane steam reforming reaction, a different reactivity order is reported in the literature.^{119–122} A general trend shows the following order of reactivity: Rh,Ru > Ni,Ir > Pt,Pd.¹¹⁹ A comparison between the reactivity of the metal for both reactions may explain the lower susceptibility of Rh to carbon deposition during SR of ethanol.

3.1.2. Nature of the Carbon Formed. There are two general types of **carbonaceous deposits** reported in the literature: filamentous carbon and amorphous carbon. The latter may cover both the metal particles and the support.^{81,102–104} The nature of carbon formed depends on both the reaction temperature and the nature of the metal selected.

3.1.2.1. Noble Metal Catalysts. With respect to the noble metal-based catalysts, carbon formed can encapsulate the metal particles or cover the support. Both of these lead to losses in activity. The deactivation of Rh/MgO and Rh/Al₂O₃ catalysts during SR of ethanol was attributed to carbon formation.^{123,124} Transmission electron microscopy (TEM) images of the used Rh/Al₂O₃ catalyst showed the presence of amorphous carbon encapsulating the metal particles. This resulted in blocking of active metal sites.¹²⁴ The deactivation of a series of 2 wt % Rh/Ce_xZr_{1-x}O₂ catalysts during SR of ethanol at low temperature was also attributed to carbon deposition.¹⁰⁰ The decline in activity was closely correlated with the formation of ethylene, a common carbon precursor, due to its facility to polymerize. In this case, the catalyst could be completely regenerated after treatment with an O₂/He mixture above 473 K.¹⁰⁰ Some authors proposed that these **carbonaceous deposits correspond to residues of reaction intermediates**. For example, Platon et al.¹⁰¹

reported that a significant build-up of reaction intermediates occurred during the SR reaction over 2 wt % Rh/Ce_{0.8}Zr_{0.2}O₂, which could contribute to catalyst deactivation. These carbonaceous intermediates were less stable at higher reaction temperatures. They suggested that ethylene and acetone were the main intermediate products responsible for the most significant deactivation. Erdőhelyi et al.⁷⁶ proposed that the deactivation of supported noble metal catalysts was caused by the accumulation of acetate-like species over the support. They suggested that these species inhibited the migration of ethoxy species from the support to the metal particles and, thus, hindered their decomposition. The stability of these surface acetate species was found to depend on the support.¹²⁵ The addition of zirconia to alumina favored the decomposition of acetate species and increased the selectivity to H₂. de Lima et al.³⁹ reported that DRIFTS spectra recorded during SR of ethanol at 773 K over CeZrO₂ and 1.5 wt % Pt/CeZrO₂ revealed the presence of bands attributed to acetate species (Figure 16). The DRIFTS spectra of CeZrO₂ showed that the

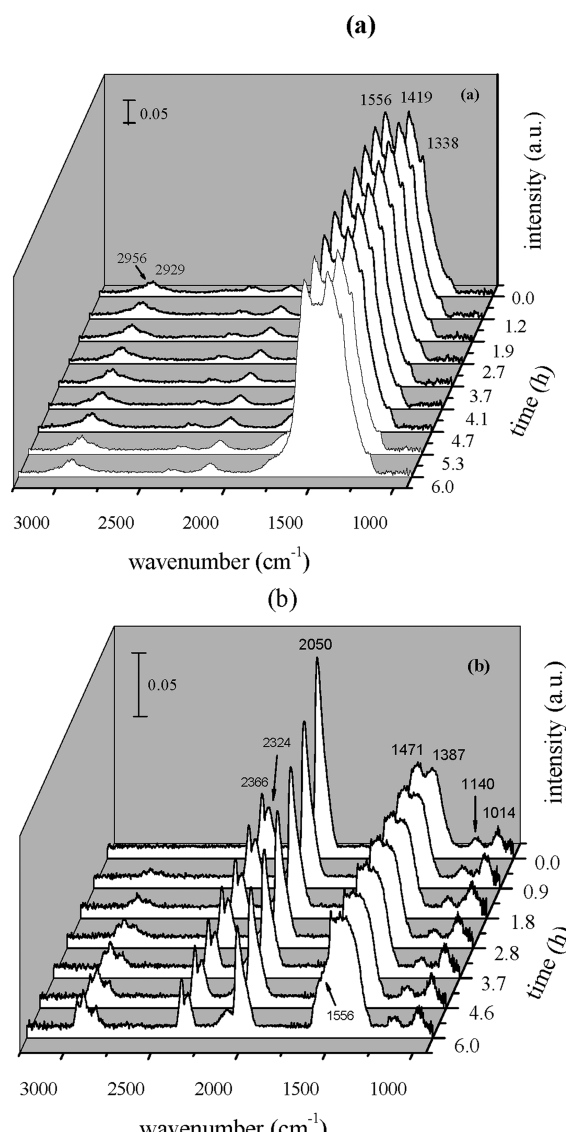


Figure 16. DRIFTS spectra obtained over (a) CeZrO₂ and (b) Pt/CeZrO₂ at 773 K and under the reaction mixture containing ethanol and water (water/ethanol ratio = 2.0) during 6 h TOS. Reprinted with permission from ref 37. Copyright 2008 Elsevier.

intensities of these bands remained unchanged during the reaction. However, in the case of Pt/CeZrO₂, an increase in the intensities of the bands assigned to the acetate species was accompanied by decreases in those bands corresponding to CO adsorbed on Pt and gas-phase CO₂. This suggests that the rate of decomposition of acetate species decreased during the reaction and, hence, led to their accumulation on the catalyst surface. On the other hand, unpromoted CeZrO₂ exhibited high surface coverages of adsorbed acetate species at 773 K but did not lose activity during the reaction. Therefore, the accumulation of acetate species on the Pt/CeZrO₂ catalyst surface seems to be symptomatic and not the root cause for the deactivation of the Pt/CeZrO₂ catalyst. The authors have proposed that the unbalance between the rate of the decomposition of acetate species to CO and CH_x species and the rate of desorption of CH_x species as CH₄ leads to the accumulation of carbon deposits. This in turn obstructs the Pt–support interface, which results in catalyst deactivation, because the acetate demethanation reaction is promoted by the metal. The loss of the Pt–support interface thus results in an increasing steady-state coverage of acetate species with respect to time on stream (TOS). Because an increasing coverage of acetate species on the catalyst surface reflects a growing inability to turn over the acetate intermediate, the result is an increase in acetaldehyde desorption. This can explain the high acetaldehyde selectivities with TOS that are generally observed in the literature. A similar bifunctional mechanism was reported for the steam reforming of acetic acid over a Pt/ZrO₂ catalyst.¹²⁶ The authors proposed that acetic acid decomposes to CO, CO₂, and CH_x via acetate formation at the metal–support interface and that water is activated on the support. It was suggested that the catalyst deactivates when the boundary sites between Pt and zirconia are blocked by CH_x residues.

The decomposition of dehydrogenated species (acetaldehyde and/or acetyl species) can also contribute to the accumulation of CH_x species. This in turn leads to the gradual obstruction of the Pt–support interface with time onstream and ultimately results in catalyst deactivation. This reaction is typical of the metallic phase and could also explain the absence of deactivation over unpromoted CeZrO₂.

3.1.2.2. Ni- or Co-Based Catalysts. A number of characterization techniques (e.g., Raman spectroscopy, temperature-programmed oxidation (TPO), and TEM) revealed the formation of filamentous carbon in addition to amorphous carbon on Ni- or Co-based catalysts.^{26,81,102–104,127} For instance, TEM images of a deactivated Co/ZnO catalyst after SR showed Co particles either covered by carbonaceous deposits or located within carbon filaments (Figure 17).⁸¹

The mechanisms of carbon formation and the growth of filaments for steam reforming and the decomposition of methane over supported Ni catalysts are well-described.^{113–115} Methane dissociates on the nickel surface, and this produces highly reactive carbon species.¹¹³ This carbon can undergo a number of processes, including (i) reaction with water; (ii) encapsulation of the Ni particle surface; or (iii) dissolution into the Ni crystallite followed by the nucleation and growth of carbon filaments (e.g., whiskers). However, few studies have been dedicated to studying the carbon formation mechanism for ethanol steam reforming. A similar mechanism was proposed for the growth of filamentous carbon as a result of the decomposition of ethanol on Ni foams.¹²⁸ The temperature of the ethanol decomposition as well as the Co loading significantly affected the growth of multiwalled carbon

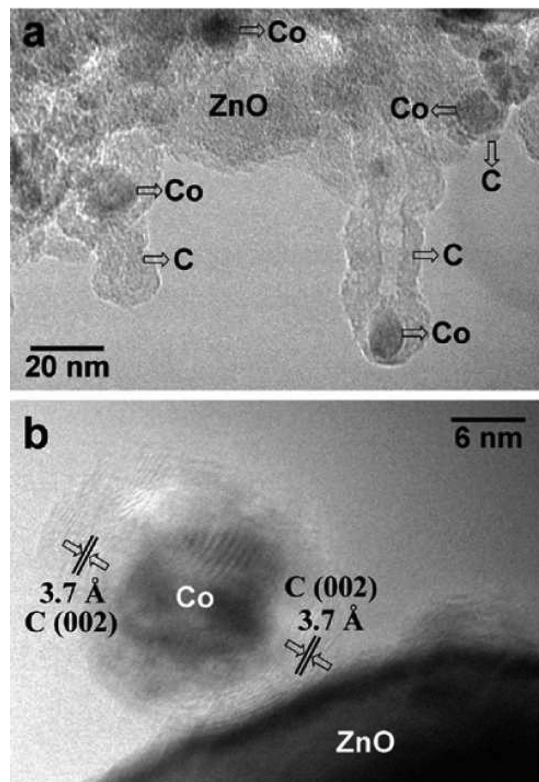


Figure 17. Transmission electron microscopy images corresponding to the deactivated Co/ZnO. Reprinted with permission from ref 81. Copyright 2005 American Chemical Society.

nanotubes (MWCNT) on Co/C catalysts.¹²⁹ Increasing the reaction temperature did not favor the formation of CNT.

According to the reaction mechanism proposed for the SR of ethanol, the decomposition of dehydrogenated species (e.g., ethoxy, acetaldehyde, acetyl) and acetate species all produce hydrogen, CO, and CH_x species, which can in turn result in carbon formation depending on the rate of hydrogen recombination.³⁸ Therefore, when the rate of this reaction pathway is higher than the rate of desorption of CH_x species as CH₄, the catalyst should deactivate. This is because the CH_x species formed can block the metal surface. The CH_x species can be further dehydrogenated to form H and C. In the case of Ni- or Co-based catalysts, this highly reactive carbon species has several options; it can (a) react with O₂ (or H₂O) to produce CO_x species; (b) encapsulate the Ni or Co particle; or (c) diffuse through the Ni or Co crystallite and nucleate the growth of carbon filaments (Figure 18). It should be borne in mind that the metal (Ni or Co) can remain active during the SR of ethanol despite having a considerable amount of carbon deposited behind the particles. This is because the top surface still remains exposed to the reactants and gas-phase intermediates.^{38,130} According to Trimm,¹³¹ this is a special case where the coke formed does not necessarily result in catalyst deactivation.

A similar carbon formation mechanism was reported for bimetallic catalysts. DRIFT spectra were recorded by Sanchez-Sanchez et al.¹³² over 2.5 wt % Pt/Al₂O₃, 13 wt % Ni/Al₂O₃, and 2.5% Pt 13% Ni/Al₂O₃ catalysts under ED and SR of ethanol at 400 °C. They observed that adsorbed species developed over the Pt/Al₂O₃ catalyst during SR of ethanol. For all the catalysts studied, the DRIFT spectra at room

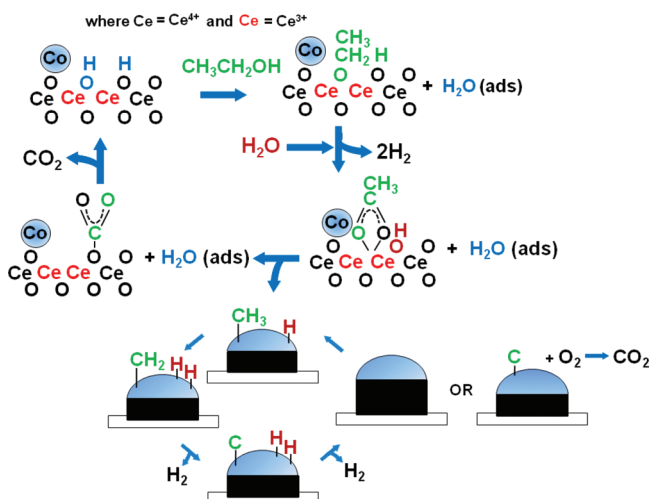


Figure 18. Reaction mechanism proposed for the ethanol conversion reactions over Co-based catalysts. Reprinted with permission from ref 38. Copyright 2008 Elsevier.

temperature showed bands corresponding to the $\nu(\text{CO})$ modes of linearly and bridged-bonded CO adsorbed over metallic sites. The intensities of these bands decreased with TOS, whereas the intensities of the bands associated with acetate and carbonate species increased and eventually became the main bands. These changes in band intensities were attributed to the deactivation process occurring on the active sites, which are responsible for the decomposition of the acetaldehyde intermediate into CO and CH_4 . The authors suggested that the first reaction pathway of SR of ethanol over the three catalysts studied was ethanol dehydrogenation followed by decomposition of the acetaldehyde formed. This decomposition takes place over the metallic sites, which are quickly deactivated by the formation of carbon deposits. These are most likely derived from the methyl groups arising from C–C bond-breaking reactions and from polymerization of the ethylene species produced from ethanol dehydration. It was proposed that the main reaction pathway operating in SR of ethanol involves the decomposition of acetate species formed over the alumina surface, which accumulates with TOS. The authors proposed that the improved stability of the bimetallic catalyst is due to the enhanced ability of Ni to gasify the methyl groups formed as a result of the decomposition of the acetate species. In the case of the monometallic catalysts, these methyl groups are dehydrogenated to carbon. This proposed mechanism is in good agreement with previous studies that examined ethanol conversion reactions over noble metal^{37,39} and transition metal³⁸ based catalysts.

The type of carbon formed on Ni- or Co-based catalysts depends on the reaction conditions (e.g., reaction temperature, steam-to-ethanol molar ratio, and oxygen-to-ethanol molar ratio) and the nature of the support. Llorca et al.¹²⁷ carried out a comprehensive study of the nature of carbon deposition during the SR of ethanol on 1 wt % Co supported over different oxides (i.e., Al_2O_3 , SiO_2 , MgO , TiO_2 , V_2O_5 , ZnO , La_2O_3 , CeO_2 , and Sm_2O_3). Regardless of the type of support used, carbon deposits covering the support as well as metallic particles were identified. The extent and degree of ordering of the carbon formed depended on the support and the reaction temperature. Increasing the reaction temperature increased the amount of

carbon deposited, as well as the degree of order of the carbonaceous phase. For a Co/ZnO catalyst, TEM analysis revealed the presence of metallic cobalt particles covered by a poorly ordered carbonaceous phase after reaction at 723 K. In addition, following reaction at 873 K, carbon filaments containing Co particles at the tip were also detected. Wang et al.¹⁰⁴ investigated the deposition of carbon during SR over Co/CeO_2 as a function of reaction temperature. Severe deactivation was observed at 623 and 723 K. In this case, the cobalt particles were found to be completely encapsulated by coke. When the reaction was carried out at 773 or 823 K, carbon filaments were detected but the catalyst remained quite stable for 8 h of TOS. Above 873 K, carbon deposits were no longer detected by TEM analysis. Galetti et al.¹⁰³ also studied the effect of the SR reaction temperature on the performance of a CuCoZnAl catalyst (11.3 wt % Co, 12.2 wt % Cu, 25.1 wt % Zn, and 20.7 wt % Al) prepared by the coprecipitation method. CuCoZnAl rapidly deactivated during SR at 673 and 773 K. At 873 K, however, the activity remained unchanged. Scanning electron microscopy (SEM) confirmed the presence of carbon filaments after reaction at 773 K, while amorphous carbon was observed at 873 K. They proposed that coke was removed from the surface of the catalyst by the reverse of the Boudouard reaction, which led to an improvement in catalyst stability at higher temperatures (i.e., 873 K). Zhang et al.²⁶ compared the stability of 15 wt % Co/CeO_2 and 15 wt % Ni/CeO_2 catalysts for the SR of ethanol at different reaction temperatures. At lower reaction temperatures (e.g., 723 and 773 K), both catalysts deactivated; the hydrogen selectivity significantly decreased, and acetone was observed. The authors correlated the deactivation to the appearance of acetone. At higher reaction temperatures (e.g., 923 and 973 K), Co/CeO_2 remained stable for a longer period of time while Ni/CeO_2 significantly deactivated. HR-TEM images revealed that deactivation was accompanied by the formation of filamentous carbon as well as metal particle sintering. The deactivation of a NiRh/CeO_2 catalyst (5 wt % Ni and 1 wt % Rh) during OSR at a low temperature of 623 K was also attributed to the poisoning of the catalyst surface by the reactants and/or products.¹³³ It is worth noting that, at higher reaction temperatures (e.g., 723 and 873 K), the catalyst was quite stable. This is most likely due to the more facile desorption of these species.

TEM images were obtained after subjecting the catalyst to different reaction conditions with the aim of shedding light on the nature of the carbon formed over 10 wt % Co/CeO_2 .³⁸ The images of the Co/CeO_2 catalyst following exposure to SR and OSR at 773 K are shown in Figure 19 a and 19 b. They reveal the presence of carbon nanofibers or filaments. Carbon nanostructures were not detected over the Co/CeO_2 catalyst following SR at 1073 K (Figure 19 c). In this case, some regions revealed only the presence of amorphous carbon in proximity to the ceria agglomerates. The absence of significant carbon deposits during SR at high temperature was attributed to (i) the steam and CO_2 reforming of methane reactions; (ii) the reverse of the disproportionation reaction; and/or (iii) the carbon gasification reaction, all of which are favored at high temperatures.

Increasing the water-to-ethanol molar ratio also improved the stability of a $\text{Ce}_2\text{Zr}_{1.5}\text{Co}_{0.5}\text{O}_{8-\delta}$ catalyst (prepared by a sol–gel method) during SR of ethanol. In addition, it increased the amount of filamentous carbon formed.¹³⁴ These results indicate that filamentous carbon was not responsible for the deactivation of the catalyst. According to the authors, the acetate and

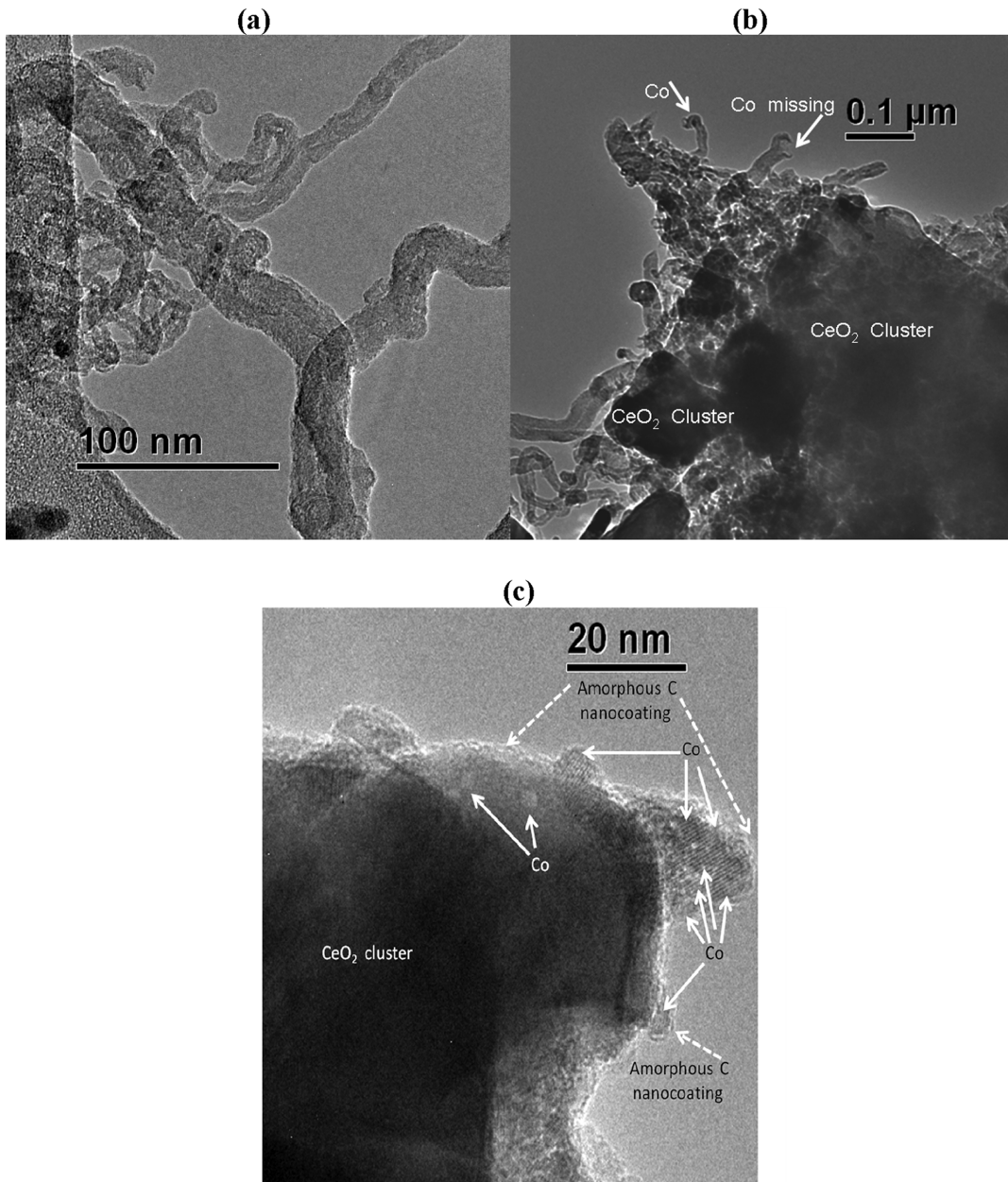


Figure 19. HR-TEM images of the Co/CeO₂ following different reaction conditions: (a) SR under H₂O/ethanol molar ratio = 3.0 at 773 K; (b) OSR under H₂O/ethanol molar ratio = 3.0 and O₂/ethanol molar ratio = 0.5 at 773 K; (c) SR under H₂O/ethanol molar ratio = 3.0 at 1073 K. Reprinted with permission from ref 38. Copyright 2008 Elsevier.

carbonate species formed on the catalyst surface during the reaction prevented the adsorption of ethanol and water, and it was this competition for the same active sites that resulted in catalyst deactivation.

For solid oxide fuel cells (SOFC), the water-to-ethanol molar ratio is particularly critical. In this case, pure ethanol (water-to-ethanol molar ratio = 0) can be directly used as a fuel without the need for either ethanol reforming to hydrogen or hydrogen purification. This results in a significant decrease in both the complexity and the cost of the fuel cell system.¹³⁵ Ni/YSZ cermet materials are commonly used as anodes in SOFC. Ni provides electrical conductivity and catalytic activity for the reforming reactions in the SOFC anodes. The latter produce hydrogen and carbon monoxide, which are, in turn, consumed electrochemically, with the simultaneous generation of

electricity.¹³⁶ However, to reach the percolation threshold for electrical conductivity, a high Ni content (at least 30 vol %) is necessary. Unfortunately, this high Ni content leads to excessive carbon formation and, hence, a rapid decline in cell performance. In order to establish the carbon deposition boundaries to avoid the deactivation of SOFC fuelled by pure ethanol, some authors¹³⁷ evaluated the thermodynamics of carbon formation as a result of ethanol decomposition. Their results indicated that carbon was formed over the entire temperature range studied (773–1173 K). Increasing the temperature decreased the amount of carbon formed at equilibrium, with the level stabilizing at 20 mol % above 1123 K. At this temperature, ethanol has essentially completely decomposed to H₂, CO, and C. Significant carbon deposition was detected on Ni-based anodes of SOFC running directly

on pure ethanol.¹³⁵ Therefore, alternative materials that exhibit high catalytic activity for ethanol conversion as well as adequate ionic and electronic conductivities and carbon resistance have been proposed as anode materials for SOFC. These include Ni supported on ceria-based oxides such as gadolinium- or zirconium-doped ceria.^{138–143}

Bichon et al.¹³⁰ followed the evolution of carbon deposits during SR over Ni/Al₂O₃, Co/Al₂O₃, Co/TiO₂, and Co/SiO₂ catalysts. Thermogravimetric analysis revealed that the amounts of carbon deposited after 8, 24, and 48 h of TOS were similar, thus demonstrating that carbon deposition appears to take place at the beginning of the reaction.

3.1.3. Effect of Ethanol Purity on Carbon Formation (Bioethanol). Bioethanol or crude ethanol can be obtained from different biomass feedstocks such as corn and sugar cane (first-generation bioethanol) or agricultural residues (second-generation bioethanol).¹ The ethanol production processes involve the conversion of biomass into fermentable sugars, which then undergo fermentation. To produce ethanol as a fuel suitable for blending with gasoline, water has to be removed above the azeotropic levels. Pure ethanol is produced in a multistep distillation, which removes the contaminants and water. However, SR of ethanol requires that water be added to the process. Therefore, the use of crude bioethanol as the feedstock for hydrogen production could eliminate the need for the energy-intensive distillation steps. This would make the SR process much more attractive from a cost standpoint. The crude ethanol obtained, depending on the feedstock used and the degree of purification, contains various impurities such as esters, aldehydes, higher alcohols, acids, and sugars. However, the presence of impurities in the feed can change the hydrogen yield and/or contribute to catalyst deactivation.

The majority of studies on SR of ethanol reported in the literature were based on the use of water and pure ethanol mixtures, obtained by mixing distilled ethanol with water. Few were dedicated to the production of hydrogen by the SR of bioethanol.^{102,144–146} Vargas et al.¹⁰² studied the performance of a Ce₂Zr_{1.5}Co_{0.5}O_{8-δ} catalyst for the SR of both pure ethanol and bioethanol obtained by the fermentation of sugar cane molasses followed by simple distillation. The resulting bioethanol was found to contain traces of methanol, *n*-propanol, *n*-butanol, and isoamyllic alcohol. The catalyst rapidly deactivated during SR due to the formation of amorphous and filamentous carbon, irrespective of the feed used. However, significant differences in the degree of deactivation in either case were not observed. le Valant et al.¹⁴⁴ investigated the effect of different impurities in bioethanol during SR over a 1 wt % Rh/MgAl₂O₄ catalyst. These impurities caused two different effects on the ethanol conversion: diethylamine and butanal favored ethanol conversion, whereas the presence of butanol, diethylether, and ethyl acetate induced a poisoning effect, mainly due to carbon deposition. For example, diethylamine is a basic molecule that adsorbs preferentially on the acid sites of the support. This inhibits the dehydration reaction that leads to the production of ethylene. On the other hand, the deactivation by ethyl acetate was attributed to its strong adsorption onto the support, which in turn hinders the adsorption of ethanol onto the catalyst surface.

3.1.4. Strategies for Minimizing Carbon Formation.

The different approaches used to reduce carbon formation are based on either the prevention of carbon formation reactions in

the first place or on the rapid conversion of carbon, once formed, to gaseous products for ease of removal.

3.1.4.1. Increasing the Steam/Ethanol Ratio. By increasing the steam-to-ethanol molar ratio of the feed, the formation rate of the carbon is decreased and this improves catalyst stability.^{16,17,134} Increasing the steam-to-ethanol molar ratio of the feed aims at promoting the gasification of carbon by water (eq 23), and this, in turn, decreases the catalyst deactivation rate through continuous carbon removal. DRIFTS studies revealed that water promotes the decomposition of the acetate species and releases hydrogen in the process.^{37,39} Steam-to-ethanol molar ratios ranging from 0 to 15 have been reported in the literature. However, an excess of water results in higher operating costs due to a less energy-efficient plant as a result of increased utility costs for producing the steam. Furthermore, the effectiveness of this strategy depends on the rate of the gasification reaction ultimately achieved by the catalyst. In general, this has been slow.¹³¹ For example, a 2 wt % Rh/CeZrO₂ catalyst underwent significant deactivation during SR even at a high steam-to-ethanol molar ratio of 8.0.¹⁰⁰ The effect of the H₂O-to-ethanol molar ratio on the performance of a 1.5 wt % Pt/CeZrO₂ catalyst during SR was also investigated. Increasing the H₂O-to-ethanol molar ratio from 2.0 to 10.0 decreased the catalyst deactivation rate. However, this was still not enough to achieve long-term catalyst stability.³⁹ A decrease in the amount of carbon deposited on a 10 wt % Co/CeO₂ catalyst surface following SR at 773 K occurred when the steam-to-ethanol molar ratio was increased from 3.0 to 10.0.³⁸

3.1.4.2. Adding Oxygen to the Feed. To avoid carbon deposition during the SR reaction, one strategy adopted has been the addition of oxygen to the feed as has been employed for OSR^{6,18,19,24,36–39,106,124,133,147–156} and POX.^{82,83,157–162} According to the literature, oxygen from the feed enhances the gasification rate of the carbon deposits formed, and this improves catalyst stability.

By comparing the amount of carbon formed during the SR and OSR of ethanol over 21% Ni/MgO and 30% Ni/CeO₂ catalysts, the rate of carbon formation was found to be significantly reduced in the presence of oxygen (Figure 20).

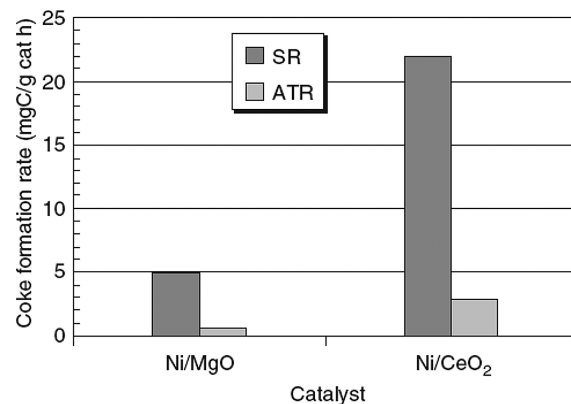


Figure 20. Coke formation rate in SR and ATR conditions: $T = 650\text{ }^{\circ}\text{C}$, $\text{GHSV} = 40\ 000\text{ h}^{-1}$. Reprinted with permission from ref 106. Copyright 2006 Elsevier.

In addition, the nature of the carbon formed appeared to be affected by the reaction conditions. Filamentous carbon and amorphous carbon were formed during SR, whereas filamentous carbon was not detected following OSR.

The authors suggested that the carbon formed was rapidly oxidized to CO_x . This prevented its diffusion through the Ni particles, thus hindering the nucleation of the carbon filaments.

The oxygen-to-ethanol molar ratio significantly impacted the amount of carbon formed during OSR over 5.0% Ni/CeO₂ and 5.0% Ni/Al₂O₃ catalysts.¹⁴⁷ Increasing the oxygen-to-ethanol molar ratio decreased the amount of carbon deposited for both catalysts. For a Ni/CeO₂ catalyst, carbon was no longer detected at an oxygen-to-ethanol molar ratio of 0.4, whereas carbon deposits were still present even under a high oxygen-to-ethanol molar ratio of 1.0 for the Ni/Al₂O₃ catalyst. The high resistance of Ni/CeO₂ to carbon deposition was explained in terms of the oxygen storage capacity of ceria. The highly mobile lattice oxygen reacts with the hydrocarbons formed, thus preventing the accumulation of carbon deposits. It was suggested that the oxygen vacancies of the support were regenerated by oxygen or steam from the feed.

de Lima et al.^{37,38} carried out a comparative study of SR, POX, and OSR of ethanol over two catalysts: 1.5 wt % Pt/CeZrO₂ and 10 wt % Co/CeO₂ catalysts. They also examined the effects of the reaction conditions on catalyst deactivation rates. Both catalysts significantly lost activity during the SR reaction. On the other hand, it was found that for the POX and OSR reactions the stability of both catalysts improved. With the Co-based catalyst, the amount of carbon deposited after the SR reaction (4.3 mg_{carbon/g_{catal}}/h) was higher than that observed after either a POX (1.8 mg_{carbon/g_{catal}}/h) or OSR (1.5 mg_{carbon/g_{catal}}/h) reaction. The carbon formed will either (a) diffuse through the metal to assist in carbon filament growth or (b) react with O₂ to produce CO_x species. The oxygen can either come from the support near the metal particle (i.e., the support would be replenished by the gas-phase oxygen) or directly from the feed. The result is that the high oxygen storage/release capacity of the Co/CeO₂ catalyst promotes the mechanism of continuous removal of carbonaceous deposits from the active sites, thus keeping them active for a longer period of time. The metal can remain active despite having a considerable amount of carbon deposited behind the particles because the top surface remains exposed to reactants and gas-phase intermediates.

3.1.4.3. Cofeeding CO₂. The CO disproportionation reaction (eq 18), otherwise known as the Boudouard reaction, is an exothermic reaction and, as a result of thermodynamic limitations, becomes less important at high temperatures. Galetti et al.^{103,163} reported that the reverse of the Boudouard reaction becomes significant above 873 K. As a result, it contributes to the removal of carbon, thereby increasing the catalyst resistance to deactivation.

However, the Boudouard reaction can contribute to carbon deposition during the low-temperature SR of ethanol reaction. In this case, the addition of CO₂ to the feed can shift the equilibrium in favor of the reactants and help to diminish carbon formation.

The addition of CO₂ was found to significantly improve the stability of a Pt/CeO₂ catalyst during the SR of ethanol at 773 K.¹⁶⁴ DRIFTS spectra for a mixture containing ethanol, water, and CO₂ at different temperatures revealed that CO₂ competes with ethanol for the same adsorption sites. This leads to a reduction in the rate of decomposition of the adsorbed intermediate species. This directly impacts on the rate of CH_x species formation, thereby alleviating catalyst deactivation.

It is noteworthy that, in the absence of steam, the reaction between ethanol and CO₂ (i.e., dry reforming (DR) of ethanol) strongly favors the formation of carbon.^{165–167} It is only at high reaction temperatures and high CO₂-to-ethanol molar ratios that the carbon formation reactions become thermodynamically unfavorable.¹⁶⁵ da Silva et al.¹⁶⁷ investigated the CO₂ reforming of ethanol over a 1.0 wt % Rh/CeO₂ catalyst. Regardless of the CO₂-to-ethanol molar ratios employed, during DR of ethanol at 773 K, the catalyst was found to significantly deactivate due to carbon deposition. At this temperature, the ethanol decomposition reaction is most likely taking place along with methane production. However, CO₂ reforming of the methane formed appears to occur only to a limited extent under these conditions. Increasing the reaction temperature from 773 to 1073 K greatly improved the stability of the catalyst because the methane dry reforming reaction is favored at high temperatures.

3.1.4.4. Catalyst Modification. The nature of the support can also strongly influence the stability of the catalyst during SR because it is found to independently exhibit activity for this reaction. The support can play another major role in the SR of ethanol by assisting in the removal of carbon or suppressing its formation. To increase the rate of the carbon gasification reaction by either favoring water adsorption or neutralizing the acid sites responsible for ethylene polymerization, several studies were dedicated to modifying the acid/base properties of the support through the addition of dopants such as alkali metals,^{78,100,124,168,169} alkaline earth metals,^{79,152,170} or rare earth oxides.^{15,171–174} However, it should be noted that the addition of dopants can impact the electronic properties of the metal or block or modify specific adsorption sites.

Sodium addition (0–1 wt %) to a 10 wt % Co/ZnO catalyst improved the stability of the catalyst for the SR of ethanol.¹⁶⁸ In the absence of sodium, Co/ZnO strongly deactivated due to the abundant deposition of carbon.¹⁷⁵ Increasing the sodium content inhibited carbon deposition and significantly decreased catalyst deactivation. The authors suggested that sodium promoted the removal of CH_x species produced from C–C bond-breaking reactions. These are considered to be the precursors of carbon deposition. The authors noted that, with nickel catalysts, potassium reduces graphite formation by blocking step sites but at the same time facilitates the gasification of carbonaceous residues. Therefore, in this particular case, it is not clear whether the alkali modifies the metal, the support, or both.

Doping Ni/MgO with potassium was also found to inhibit the formation of carbon filaments. It was proposed that this is due to electronic enrichment of the metal particles (Figure 21). It was also suggested that this suppresses the Boudouard reaction as well as the hydrocarbon decomposition activity.¹²⁴ Therefore, carbon diffusion through the Ni particles is most likely limited, because the concentration of carbon on the Ni metal surface was deemed to have been kept low. Thus, in this case, the proposed advantage of the alkali is associated with the modification of the metallic function.

However, the addition of 0.5 wt % of potassium to a Rh/CeZrO₂ catalyst was found to only slightly improve the ethanol conversion; the catalyst still underwent significant deactivation.¹⁰⁰ Adding more K (5 wt %) strongly decreased the activity of the catalyst. It has been postulated that alkali compounds such as potassium can neutralize the acid sites of alumina,

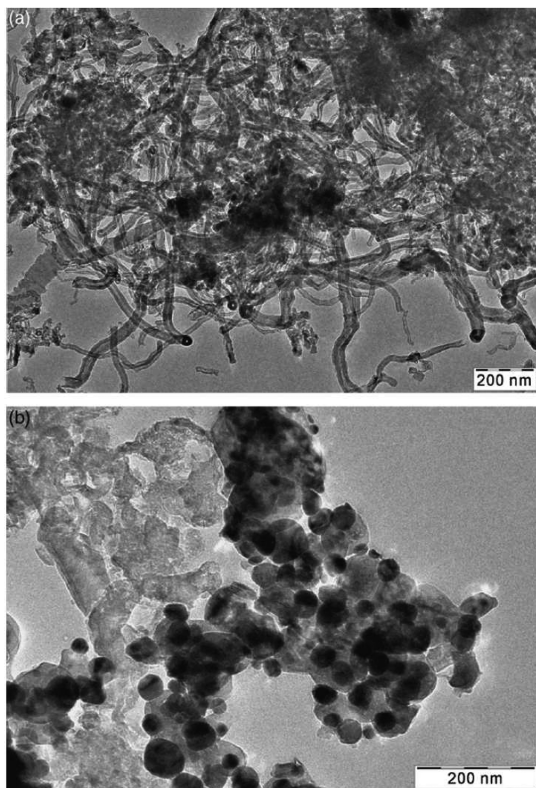


Figure 21. Steam reforming of ethanol: TEM images of Ni/MgO aged catalysts: (a) undoped Ni/MgO and (b) K-doped Ni/MgO. Reprinted with permission from ref 124. Copyright 2007 Elsevier.

thereby decreasing the formation of ethylene and, hence, coke formation. In addition, Domök et al.⁷⁸ suggested that adding K to 1 wt % Pt/Al₂O₃ lowers the stability of the acetate species, thus reducing its poisoning effect and improving catalyst stability. The authors remark that the question remains open as to how the K additives bind to the support influence the reaction occurring on Pt.

Carrero et al.¹⁷⁰ studied the effect of the addition of Mg and Ca on carbon formation over a NiCu/SiO₂ catalyst (2 wt % Ni and 7 wt % Cu) during SR. The incorporation of Ca and Mg (5 and 10 wt %) significantly reduced the amount of carbon deposited. In addition, Raman spectroscopy revealed the formation of less ordered carbon on Ca- and Mg-promoted catalysts. This less-ordered carbon is more reactive and thus more easily removed by gasification during SR; hence, a decrease in the extent of carbon deposition is achieved.

The addition of rare earth oxides (Sc, Y, La, Er, and Gd) to 1 wt % Rh/Al₂O₃ induced several changes in the acid–base properties of the support: (i) a decrease in the concentration of stronger Lewis acid sites; (ii) the appearance of new Lewis acid sites of weaker strength; and (iii) an increase in the surface basicity.¹⁷⁴ Therefore, the incorporation of these rare earth oxides resulted in lower production of ethylene and, consequently, less carbon deposits.

The addition of La₂O₃ to a Ni/Al₂O₃ catalyst significantly decreased the rate of carbon deposition due to the coverage of the acidic sites of alumina by the basic lanthana species. These acid sites are responsible for the dehydration reaction.¹⁵ Fatsikostas et al.¹⁶ proposed that the LaO_x species formed during reduction could react with CO₂ to produce La₂O₂CO₃.

This lanthanum oxycarbonate species can react with carbon to form CO and regenerate La₂O₃ by promoting the removal of carbon. The presence of these LaO_x patches over the surface of the Ni particles was proposed as the reason for the suppression of CO adsorption on the Ni particles of the Ni/La-Al₂O₃ catalysts.¹⁷¹ In this case, the addition of lanthana was found to decrease the rate of formation of carbon during SR of ethanol. The lanthanum oxide is proposed as being located as patches on the surface of the nickel rather than on the support.

Sanchez-Sanchez et al.¹⁷² studied the effect of the addition of different metal oxides (5% La₂O₃, 2.5% MgO, 7.0% ZrO₂, 8.4% CeO₂) on the performance of Ni/Al₂O₃ for SR of ethanol. All the metal oxides added decreased the acidity of the alumina, but carbon deposits were still detected in all of the catalysts studied. The amount and the nature of the carbon formed varied as a function of the metal oxide added. For the Ni/La-Al₂O₃ and Ni/Ce-Al₂O₃ catalysts, the formation of carbon filaments was significantly reduced, and this was attributed to the coverage of the metallic nickel particles by ceria and lanthana species. Thus, the authors propose that in this case the oxides cover both the support, which suppresses the acidity, and the nickel particles, where it is suggested they suppress the growth of the carbon filaments.

Recently, an increasing number of papers report the use of ceria and ceria-containing mixed oxides as a support for the SR and OSR of ethanol.^{1,6,18,26,36–39,42,76,79,80,97,100,102,104,106,108,133,147,153,164,167,176–184} Redox supports such as ceria and ceria-containing mixed oxides improve catalyst stability due to their high oxygen storage capacity (OSC) and oxygen mobility. The oxygen-exchange capacity of cerium oxide is associated with its ability to reversibly change oxidation states between Ce⁴⁺/Ce³⁺ by storing/releasing oxygen.¹⁸⁵ This highly mobile oxygen can react with carbon species as soon as it forms, and this keeps the metal surface free of carbon, thus inhibiting deactivation. However, it should not be assumed that a change in oxidation state of ceria is automatically required if the oxygen is supplied by the dissociation of H₂O at O-vacancy sites, which form defect-associated bridging OH groups. In this case, the ceria atoms associated with the –OH groups can remain in the Ce³⁺ oxidation state (e.g., during the SR of ethanol). The case of adsorbed O adatoms formed from the dissociation of O₂ at O-vacancies would likely require a change in oxidation state of ceria from Ce³⁺ to Ce⁴⁺ (e.g., during POX of ethanol).

A 2 wt % Ir/CeO₂ catalyst was found to remain quite stable during SR, POX, and OSR of ethanol at 923 K.³⁶ Deactivation was not observed for any of the reaction conditions studied. Catalyst stability was attributed to the carbon removal mechanism that takes place at the metal–support interface. It was proposed that the carbon formed caused the oxide support near the metal particle to be partially reduced. Thus, the OSC of ceria probably promotes the carbon gasification reaction by inhibiting the catalyst deactivation. No deactivation was observed on a 1 wt % Rh/CeO₂ catalyst during the OSR of ethanol at 923 K.¹⁵¹ These authors also proposed that ceria inhibited coke deposition through oxygen transfer from ceria to the Rh particles. This contributed to carbon removal from Rh particles. For the SR of ethanol reaction, a Rh/CeO₂ high surface area catalyst exhibited better stability than a correspondingly lower surface area catalyst. This was attributed to a greater surface fugacity of available O from the support, which, in turn, could react with and remove carbonaceous species.¹⁶⁷ For a series of Rh/Ce_xZr_{1-x}O₂ catalysts tested for

the SR of ethanol reaction at low temperatures, the deactivation rate decreased as the Ce/Zr ratio increased. This was explained by an increased oxygen storage capacity as the cerium content was increased.¹⁰⁰ The incorporation of ZrO₂ into the CeO₂ lattice increases the density of oxygen vacancies in the support due to the higher oxygen mobility of the solid solution formed.¹⁸⁵ The higher the amount of mobile lattice oxygen near the metal particles, the more efficient the mechanism of carbon removal from the metallic surface.

da Silva et al.¹⁸³ investigated the effect of support reducibility on the stability of 10 wt % Co/CeO₂ catalyst for the OSR of ethanol. A significant amount of carbon was formed over Co/CeO₂-LS (low surface area ceria) whereas carbon deposits were not detected over Co/CeO₂-HS (high surface area ceria) during the reaction. DRIFTS data taken during adsorption of ethanol showed the formation of acetate intermediate species. This demonstrates the ability of the support to donate oxygen. Because there was no oxygen in the feed, the oxidation of ethoxy into acetate species must have been supplied by oxygen from the support. In addition, the formation of acetate intermediate species was favored on high surface area ceria. This indicates that the Co/CeO₂-HS catalyst displayed a greater oxygen availability compared to its low surface area Co/CeO₂-LS counterpart; this is in agreement with the oxygen storage capacity measurements. Therefore, the higher oxygen mobility of high surface area ceria promotes the mechanism of carbon removal, which in turn contributes to the greater stability of Co/CeO₂-HS. In the presence of oxygen, support vacancies can be replenished, and this keeps the cleaning mechanism operating efficiently. Song and Ozkan⁸⁰ also observed in the DRIFTS spectrum the presence of acetate species even at room temperature after ethanol adsorption over a Co/CeO₂ catalyst. This was attributed to the availability of oxygen from the ceria support. They also suggested that the high oxygen mobility of ceria suppresses carbon deposition over Co/CeO₂ and maintains a clean particle surface.

Ceria-based oxides (e.g., gadolinium- or zirconium-doped ceria) have also been used in the composition of SOFC anodes to suppress carbon deposition.^{138–142} Ceria exhibits a mixed ionic and electronic conductivity that enables operation of the SOFC to be carried out at lower temperatures (i.e., 873–1073 K). In addition, the presence of mobile oxygen provides a high resistance to carbon deposition during ethanol reforming reactions.

Catalyst modification by the addition of a second metallic element may also contribute to the reduction of carbon formation. Fierro et al.¹⁹ compared the performance of Ni/SiO₂ and NiCu/SiO₂ catalysts for OSR of ethanol. The addition of Cu to a Ni-supported catalyst improved catalyst stability. This result was attributed to the formation of a Ni–Cu alloy that inhibited the formation of nickel carbide. This species is considered to be the precursor for the growth of carbon filaments. A Co-Me (Me = Ni, Cu) solid solution was also identified by HRTEM–EELS measurements.¹⁸⁶ The amount of carbon formed depended on the nature of the second metal and followed the order CoNi(Na)/ZnO < Co(Na)/ZnO ≪ CoCu(Na)/ZnO. However, the authors did not provide an explanation for this tendency. Similar contradictory results were observed by Romero-Sarria et al.¹⁰⁵ The addition of Rh to a Co/CeZr catalyst strongly reduced the amount of carbon formed, and the catalyst remained quite stable. On the other hand, TPO experiments revealed a higher formation of carbon filaments for a Rh–Ni/CeZr catalyst. The authors suggested

that Rh significantly improved the reduction of NiO oxide, producing large metallic particles.

3.1.4.5. Ensemble Size Control. Controlling the ensemble size aims at inhibiting carbon formation by hindering the mechanistic pathways for carbon formation during ethanol steam reforming. This approach is essentially identical to that used for preventing coke formation during methane steam reforming. The CH_x species produced by the decomposition of different intermediate species can undergo further dissociation to C and H. According to Trimm,¹³¹ the dissociation of methane to give H and C requires a defined number of sites, in other words, an ensemble. Rostrup-Nielsen¹⁸⁷ proposed a critical ensemble size, below which carbon formation does not occur. Steam reforming requires ensembles of 3–4 atoms, whereas carbon formation needs 6–7 atoms. The nickel particle size significantly influences the nucleation rate of carbon. The initiation step for carbon formation is more difficult for smaller particle sizes.¹¹⁵ Therefore, controlling the number of atoms in an ensemble will most likely suppress the coke formation rate. Although the rate of carbon formation is proposed as being lower over small metallic particles, the problem of maintaining small metal particles can be difficult at the high temperatures required for reforming.

The effect of Co particle size on the performance of carbon nanofiber supported Co catalysts for SR of ethanol was also investigated.¹⁸⁸ By decreasing the cobalt size, a significant improvement in the catalyst stability was observed. As confirmed by TEM measurements, this was caused by a significantly lower rate of carbon deposition on the smallest (<3 nm) Co particles relative to the larger ones. The lower carbon deposition rate was ascribed to a lower fraction of exposed terrace atoms. These sites have been proposed to be responsible for excessive carbon deposition on catalysts composed of relatively large (>10 nm) Co particles.

It can be concluded, therefore, that because the method selected to prepare the catalyst controls the metal particle size, it plays a key role in determining catalyst stability during SR of ethanol. The preparation route should lead to the formation of small and stable metal particles. This can be achieved by methods that promote the interaction between the metal particles and the support. However, depending on the characteristics of the support, the reduction of metal oxides (e.g., especially Ni and Co oxides) can be hindered due to strong interactions with the support. In addition, the formation of nonreducible mixed oxides such as cobalt aluminate during the calcination or activation steps can also hinder reduction. The presence of these phases can result in loss in activity because the metal is considered to be the active site for the SR of ethanol reaction. Therefore, the search for an appropriate preparation method that minimizes carbon formation may have to be a compromise between achieving smaller particles and metal oxide reducibility. Different methods of catalyst preparation have been proposed for obtaining highly dispersed metallic particles: sol-gel,^{102,133} coprecipitation,^{103,189,190} and the incorporation of metal particles inside the microporous and mesoporous channels of zeolites,¹⁹¹ molecular sieves such as SBA-15,¹⁹² and carbon nanotubes.¹⁹³

For example, the insertion of Co or Ni metal particles inside carbon nanotubes (CNT) can have a positive impact on catalyst stability. However, only a few research groups have examined the SR of ethanol over CNT supported catalysts.^{193,194} Barthos et al.¹⁹⁴ carried out the reaction at 723 K

over Mo_2C supported on CNT. In this case, hydrogen and acetaldehyde were the main products formed due to the ethanol dehydrogenation reaction. In addition, the catalyst strongly deactivated during SR, with ethanol conversion decreasing from 90 to 40% during a 13 h reaction test. Seelam et al.¹⁹³ performed the SR of ethanol over CNT-supported metal catalysts (metal = 10.1% Ni, 15.4% Co, 7.7% Pt, 9.2% Rh), but the stability was not evaluated. Thus, further research aimed at controlling the distribution of metal particles inside the CNT is necessary. One option is to vary the types and densities of the functional groups added to the CNT surfaces, thereby imparting a metal–support interaction.

Hydrotalcite (HT)-type compounds have been reported as promising precursors for SR catalysts.^{195–200} HT with the general formula $[\text{M}^{2+}_{1-x}\text{M}^{3+}_x(\text{OH})_2]^{x/3+}[\text{A}^{n-}_{x/n}]^x \cdot \gamma\text{H}_2\text{O}$ consist of brucite-like layered double hydroxides (LDH). Here, the positive charge created by the substitution of divalent cations by trivalent ones is compensated by anions in the interlayers.¹⁹⁷ After calcination, the LDH form a mixed oxide with high thermal stability as well as high specific surface area. The reduction of this mixed oxide produces thermally stable and highly dispersed metallic particles. Li et al.¹⁹⁹ reported that the reduction temperature (973, 1073, 1123, 1173 K) of Ni/Mg/Al HT-like precursor strongly affects metal oxide reducibility, sintering, and carbon formation during SR of ethanol. High reduction temperatures are required to fully reduce the Ni particles due to the strong interaction between nickel and magnesium oxide. The major drawback of this is the growth in nickel crystallite size. Within the series, the catalyst reduced at 1073 K was found to exhibit the lowest degree of carbon formation.

Mixed oxides such as perovskite-type oxides (with general formula ABO_3) are also able to produce and stabilize very small metal particles upon reduction.^{201,202} Taking into account the catalyst deactivation mechanism proposed, carbon formation could either be decreased or inhibited on these highly dispersed metal particles.^{131,187} However, only a few papers have dealt with the use of perovskite-type oxide precursor as catalysts for SR of ethanol.^{40,203,204} de Lima et al.⁴⁰ compared the performance of a Ni metal catalyst derived from a LaNiO_3 perovskite-type oxide precursor with that of a La_2O_3 -supported Ni metal catalyst prepared by the conventional impregnation method of catalyst preparation. The amount of carbon deposited during OSR at 773 K over the 23% Ni/ La_2O_3 catalyst prepared by the conventional method was significantly (i.e., 6-fold) higher than that observed for the Ni/ La_2O_3 catalysts derived from the LaNiO_3 perovskite-type oxide. The higher Ni dispersion of perovskite-derived catalysts was postulated as being responsible for the decrease in the carbon formation rate. The same result was observed by Chen et al.²⁰³ for the OSR of ethanol over Ni/ La_2O_3 and LaNiO_3 -derived catalysts. The higher resistance to carbon deposition of the reduced LaNiO_3 catalyst was attributed to the highly dispersed Ni particles and the formation of $\text{La}_2\text{O}_2\text{CO}_3$, which strongly interacts with Ni particles, thus inhibiting sintering during reaction. These results reveal that perovskite-type oxide precursors can lead to promising catalysts for SR of ethanol. In addition, the possibility of partial substitution of the cation A or B can induce significant changes in both the chemical and thermal stability,²⁰⁵ thus opening up new opportunities for better controlling metal particle size to suppress catalyst deactivation. However, there has not yet been a systematic and fundamental study that correlates the composition of the

perovskite structure with the metal particle size and catalyst stability for the SR of ethanol.

Another approach used to control the metal particle size is based on the preparation of colloidal Co nanoparticles by the thermal decomposition of $\text{Co}_2(\text{CO})_8$ in the presence of oleic acid.²⁰⁶ A series of 9 wt % Co/ SiO_2 catalysts was synthesized by the impregnation of colloidal Co particles on SiO_2 . The role of oleic acid was to control the growth and protect the particles against agglomeration. In this way, the metallic Co particle is formed without the need for calcination or reduction treatments and this inhibits sintering of the metal. The amount of carbon formed during SR of ethanol decreased as the Co particle size decreased from 7.8 to 3.2 nm, thus revealing the dependence of carbon formation on metal dispersion.

Ensemble size control can also be achieved by the addition of a second metal such as tin or rhenium (e.g., alloying), both of which have been used to prevent the formation of carbon in the naphtha reforming process.²⁰⁷ The addition of a second metallic element to a metal particle can induce changes in both catalytic and adsorptive properties. This is due either to dilution or to covering a fraction of the surface of the host metal (i.e., geometric effects). In both cases, the size of the ensemble decreases, and this inhibits the formation of carbon. For example, adding a group IB metal to a group VIII metal strongly hinders the activity of hydrogenolysis reactions that produce coke precursors.²⁰⁸

The effect of the addition of Sn (0.6 and 2.6 wt %) on the performance of 1 wt % Pt/ CeO_2 catalyst for the SR of ethanol was also studied.¹⁶⁴ Results of TPD and in situ DRIFTS revealed that the decomposition of dehydrogenated species and the steam-assisted forward demethanation of acetate species, both of which generate coke-producing CH_x species, were inhibited by incorporating Sn into the Pt particles. Therefore, the rate of accumulation of the CH_x species at the metal–support interface was suggested to be lower over the PtSn-based catalysts, thus reducing the deactivation rate of the catalyst. Unfortunately, the improved stability with PtSn came at the expense of poorer catalyst selectivity (e.g., higher acetaldehyde selectivity) relative to Pt alone. Apparently, the addition of Sn preferentially impedes the reactions requiring a relatively larger ensemble of atoms to constitute the active sites, such as the C–C bond-breaking reactions.

The addition of Cu to a Ni/ SiO_2 catalyst significantly decreased the formation of carbon during SR of ethanol.²⁸ The presence of Cu eliminated the large ensembles of Ni metal atoms that favor the formation of carbon deposits. The addition of Mo to Ni/ Al_2O_3 catalyst also decreased the amount of carbon deposited.²⁰⁹ According to the authors, Mo species prevented the growth of Ni particles, thereby improving catalyst stability.

3.2. Metal Sintering

Cavallaro et al.¹⁵⁶ did not detect the formation of carbon during OSR of ethanol over 5% Rh/ Al_2O_3 (Figure 22). They suggested that any carbon formed was either partially or completely oxidized to CO_x and H_2O from the oxygen in the feed. Since these reactions are exothermic, the heat released may lead to substantial sintering of Rh particles.

The performance of MgO-supported Pd, Rh, Ni, and Co catalysts in the SR of ethanol was also investigated.⁴⁴ TEM images of fresh and used catalysts revealed pronounced metal

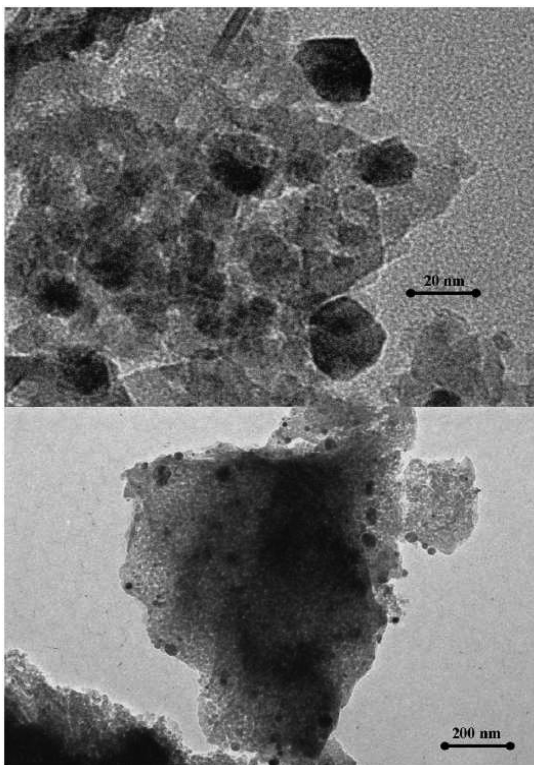


Figure 22. TEM microphotographies on the Rh/Al₂O₃ catalyst after $\tau = 100$ h in ATR conditions. O/C = 0.41 mol/mol. General conditions: S/C = 8.4 mol/mol; GHSV = 150.000 h⁻¹; $T = 923$ K. Reprinted with permission from ref 156. Copyright 2003 Elsevier.

sintering for Pd, Ni, and Co, whereas the Rh metal particle size did not change significantly during reaction. The authors correlated the deactivation of the catalyst to the sintering of the metal particles.

The support can also contribute to the stabilization of metal particles at high temperatures in the presence of steam. The metal–ceria interaction was proposed as preventing the growth of highly dispersed Ir^{26,36} or Rh¹⁵¹ particles during SR, POX, and OSR of ethanol at 923 K. Thus, the metal–support interfacial area is kept relatively constant, and this, in turn, maintains the stability of the catalysts.

3.3. Metal Oxidation

As previously discussed, adding oxygen to the feed assists in the removal of carbon formed during reaction. However, one possible side effect is oxidation of the metal particles, especially for supported transition metals, which can result in losses in steam reforming activity. de la Pena O’Shea studied the SR of ethanol over Co₃O₄ by *in situ* X-ray diffraction coupled to gas chromatography.²¹⁰ They demonstrated that ethanol dehydrogenation to acetaldehyde was the main reaction in the presence of cobalt oxide.

The lower hydrogen selectivity and higher acetaldehyde selectivity observed during OSR in comparison with SR over a Ni/CeO₂ catalyst was explained by the partial oxidation of Ni active sites.¹⁰⁶ The deactivation of a NiRh/CeO₂ catalyst (5 wt % Ni and 1 wt % Rh) during OSR at 623 K was also attributed to passivation of the catalyst surface by oxygen from the feed.¹³³ Laosiripojana and Assabumrungrat¹⁴⁷ demonstrated that there is an optimal O₂-to-ethanol molar ratio above which Ni oxidation to NiO takes place. This results in a decrease in

the reforming activity for Ni/CeO₂ and Ni/Al₂O₃ catalysts. da Silva et al.²¹¹ investigated the effect of cobalt particle size on the stability of Co supported on carbon nanofiber catalysts during OSR. The catalysts with the smallest Co particle size deactivated due to oxidation of surface atoms by oxygen from the feed. On the other hand, the catalysts having larger Co particle size (>4 nm) remained quite stable. Pereira et al.¹⁴⁸ reported that 8.3% Co/SiO₂, 4.8% Co–2.8% Rh/SiO₂ and 4.5% Co–2.4% Ru/SiO₂ catalysts all deactivated when OSR was carried out between 623 and 673 K. The decrease in ethanol conversion was accompanied by a decrease in hydrogen selectivity and an increase in acetaldehyde selectivity. Catalyst deactivation was attributed to oxidation of the surface of the Co particles by oxygen from the feed. Also, the cobalt oxide formed favored dehydrogenation of ethanol to acetaldehyde. The addition of a noble metal (e.g., Rh, Ru) was found to stabilize Co in the reduced state (i.e., the active phase for SR), thus preventing the oxidation of cobalt particles and, in turn, improving catalyst stability.

3.4. General Overview

A survey of the recent literature on catalyst deactivation during ethanol conversion reactions reveals that three main routes of deactivation have been established: carbon deposition, sintering, and oxidation of metal particles. Four side reactions responsible for carbon formation are considered to act in addition to the desired ethanol conversion reactions. At low temperatures, carbon can be formed by coking, by ethylene polymerization, or by the disproportionation of carbon monoxide (i.e., the Boudouard reaction). At higher temperatures, reverse carbon gasification and hydrocarbon decomposition reactions are the main culprits in limiting the efficacy of ethanol conversion reactions. Thermodynamic considerations indicate that carbon formation is limited to a greater extent at higher temperatures and higher oxygen-to-ethanol and steam-to-ethanol molar ratios. The acid/base properties of the catalyst are also important because suppressing surface acidity tends to hinder the dehydration of ethanol to ethylene, and this, in turn, suppresses coking by ethylene polymerization. The decomposition of hydrocarbons is not a simple matter, since numerous intermediates and byproducts (e.g., methane, ethylene, ethanol, acetaldehyde, and acetate) can either directly or indirectly lead to carbon formation. Certain metals are better able to turn over hydrocarbon molecules and, thus, tend to exhibit greater stability; one reported trend is Rh, Ru > Ni, Ir > Pt, Pd.

The structure and location of carbon deposits on the catalyst surface is a complex matter. With noble metal catalysts, carbon formation has been observed on both the metal particle and the support itself. Nowadays, noble metal catalysts are usually supported on oxides possessing high O-mobility, and both the metal and oxide components can play a direct role in the catalysis at the metal–oxide junction. In those cases, carbon buildup at the interface shuts down H-transfer reactions catalyzed by the metal. DRIFTS spectroscopy often reveals a steadily increasing inventory of O-bound intermediates on the support (e.g., acetate, carbonate). This carbon most likely results from hydrocarbon decomposition reactions. The slow desorption of CH_x species acts to increasingly squeeze the bottleneck as a function of time onstream. Although metal oxides have been reported as being less susceptible to carbon deposition, their byproduct selectivities (e.g., to acetaldehyde) are usually unacceptable.

With Ni- and Co-supported base metal catalysts, in addition to amorphous carbon, carbon exhibiting greater ordering in the form of filaments or whiskers is often found. Increasing the temperature generally increases the degree of carbon ordering. This does not necessarily result in more pronounced deactivation, however. With filaments, carbon diffuses into metal particles to nucleate the growth of filaments. These tend to lift the metal particles off the support. However, the surface at the tip of the metal particle can still remain clean and accessible to reactants. Thus, catalyst deactivation of Ni and Co catalysts should not automatically be attributed to poisoning by ordered carbon. In many cases, catalyst stability is reported to be higher at higher temperatures where ordered carbon is observed. At lower temperatures, on the other hand, the catalyst deactivates through encapsulation by amorphous coke. With Ni and Co catalysts, the application of support oxides having high O-mobility for the suppression of carbon is a generally increasing trend in the literature. However, care must be taken to avoid the formation of oxygenated byproduct such as acetone—catalyzed by the assistance of this type of metal oxide—which can poison the catalyst. Research into this category of catalyst appears promising, as a result of certain supported Co and Ni catalysts having exhibited greater stability relative to catalysts based on noble metals like Pt. Bimetallic catalysts also show promise. Nevertheless, significant carbon formation has been observed with Ni-based SOFCs, leading to the need for the design of alternative materials.

Strategies for mitigating carbon have, to date, only met with limited success. To either turn over carbon that has already formed by, for example, gasification, or to increase the ratio of oxidizing reactants (e.g., H₂O or O₂) does tend to improve catalyst stability. Although carbon deposition has been somewhat alleviated by this approach, to date long-term stability has not yet been achieved. Further drawbacks are the fact that higher steam concentrations have greater energy requirements, and adding greater amounts of oxygen typically impacts adversely on product selectivity. The addition of catalyst components (e.g., ceria, zirconia, ceria–zirconia mixed oxide, ceria–gadolinia mixed oxide) with a view to increasing the surface fugacity of oxygen (e.g., as O adatom or –OH groups) is also common. This may or may not involve a redox mechanism (i.e., a continuously changing support oxidation state), depending on the nature of the adsorbed oxygen species.

Strategies aimed at preventing carbon formation in the first place have also been applied. CO₂ cofeeding aims at suppressing the CO disproportionation reaction (the Boudouard reaction) by shifting the equilibrium in favor of the reactants. This approach has also only met with limited success. In one study, CO₂ was suggested as competing with ethanol for adsorption sites and by this means could hinder hydrocarbon decomposition reactions leading to carbon. Neutralizing acid sites by adding elements that preferentially bind to these centers may limit coking, which arises from the polymerization of ethylene. Recall that ethylene formation occurs over acid sites as a result of the dehydration of ethanol. To this end, alkali (e.g., Na and K), alkaline earth (e.g., Mg), and rare earth elements (e.g., Sc, Y, La, Er, and Gd) have all proven effective. Because coking reactions require an ensemble of 6–7 atoms to catalyze the reactions, the strategy of ensemble control is also important, because steam reforming requires a smaller ensemble of only 3–4 atoms. This can be achieved by using

methods such as nanostructuring approaches to limit the size of the metal particles. In such cases, the particles must be stabilized against sintering at the high temperatures needed for reforming. Alternatively, breaking up the ensemble either through alloying with a less-active component (e.g., group IB metal) or by selectively adding adatoms to the metal surface can be employed.

To prevent sintering, oxides that exhibit a strong enough interaction to stabilize a small metal particle size should be selected. To that end, ceria has been found to be quite effective. It should be noted that the exothermicity of the OSR or POX reactions can contribute to metal particle sintering.

On the other hand, the catalyst design and conditions used should avoid the oxidation of metal particles—another proposed deactivation route. As noted earlier, oxidation leads to a lowering in the activity and deleterious changes in product selectivities (e.g., higher acetaldehyde, less H₂). For each metal, there is an optimum oxygen-to-ethanol ratio above which oxidation of the metal occurs; this is complicated by particle size effects, with ultrasmall particles being more susceptible to oxidation. Addition of a noble metal such as Pt may assist in stabilizing base metals (e.g., Co) in a reduced state.

4. CONCLUSIONS AND SUGGESTED PATH FORWARD

Over the past decade, significant progress has been made in gaining insight into the reaction mechanisms of ethanol reforming. To this end, infrared spectroscopy has been a powerful tool in achieving this goal. In fact, although subtle differences are noted among the different research groups, remarkably good consensus has been achieved regarding the reaction pathways and catalyst structures involved in ethanol steam reforming. In general, the best supports appear to be those that are sufficiently basic to inhibit acid-catalyzed dehydration of ethanol to ethylene, which subsequently polymerizes and leads to coke formation. The dissociation of ethanol to ethoxy species can occur on the support, and those with sufficiently labile O adatoms or OH groups offer a means of accomplishing this step. Dehydrogenation of the ethoxy species to acetaldehyde is very likely assisted by the metal particles added to the support, as well as the presence of labile O adatoms or hydroxyl groups located on the support. The support also appears to provide oxygen for nucleophilic attack of the acetaldehyde species in the conversion to acetate. This step may involve O adatoms or labile OH groups (e.g., bridging type on ceria) during SR and probably O adatoms during partial oxidation. The conversion of acetate to CH₄ or its precursor and CO_x species appears to be promoted by steam and most likely involves the metal particles. Thus, both the metal particles and the support play an important role in the reaction mechanism. This is a likely case where a sufficient interface between the metal and basic support is warranted.

A major route to catalyst deactivation is that of carbon formation. In this context, knowledge gained from investigating the mechanism by infrared spectroscopy has also been fruitful. In several studies of metal/oxide catalysts, infrared spectra were collected as a function of time on stream. Steadily decreasing metal–carbonyl band intensities and steadily increasing acetate band intensities were observed. Temperature-programmed oxidation, used to characterize the nature of carbon deposits, demonstrated significant amounts of carbon deposited on the

catalyst surface. This usually included both amorphous and filamentous carbon. Taken together, the results provide interesting insight into the mechanism of catalyst deactivation. The metal appears to operate across the metal–oxide junction to assist in hydrogen transfer and related reactions such as acetate demethanation. At the same time, the intermediates appear to be bound to the oxide surface by their oxygen atoms. The metal operates on these intermediates at the metal–oxide interface. The decreasing metal–carbonyl band intensity in infrared spectroscopy is consistent with a blocking of the metal–oxide synergy, and thus, the metal gradually loses its ability to participate in the mechanism. As a result, a growing inventory of acetate and other intermediates reside on the oxide, and the selectivity of the reaction changes away from steam reforming products (e.g., H₂, CO_x) toward the desorption of unreacted intermediates (e.g., acetaldehyde).

Deactivation by coke formation is a challenging problem, especially when a noble metal such as Pt is involved. Cobalt appears to be a more promising candidate, and Co/ceria catalysts have been observed as retaining significant activity even after significant filamentous deposits have formed. Although some authors reported promising performance with Ni-containing catalysts, others observed significant deactivation due to coking.

Current and future research trends aim at accelerating the removal of carbon once formed, or minimizing the formation of carbon in the first place. The first may involve optimization of the metal ensembles, because smaller particles tend to produce less coke, or the doping of additional, less active elements into the active metal. Here, density functional theory modeling could prove fruitful in establishing the optimum particle size required or the degree of alloying required. To date, metal particle size optimization has resulted in greater success than alloying for ethanol reforming reactions. The strategy for removing carbon has generally been a two-pronged approach consisting of increasing the feed ratios of more oxidizing species (e.g., H₂O, O₂, or CO₂) and adding a metal oxide component with high oxygen mobility to increase the surface fugacities of O-containing species at the location of the carbon deposits (e.g., the metal–oxide boundary). Two additional concerns that must be addressed using these strategies include the stabilization of small particles at the temperatures required for reforming and the problem of metal particle oxidation. However, the oxidation of metal particles is more facile from a thermodynamic standpoint at smaller particle sizes. Thus, the development of nanostructured catalysts should focus on the formation of an optimized particle size range.

In addition, it should be noted that other alternatives, including liquid-phase reforming and photocatalytic reforming at near-ambient temperature, are also under development. Furthermore, most of the studies investigating SR, POX, and OSR were carried out in fixed-bed reactors using powder catalysts. The development of compact reformers could significantly contribute to reducing the costs associated with hydrogen production technologies. In this case, new catalyst formulations are needed to mitigate carbon deposition because highly active catalysts are required at very low contact times.

AUTHOR INFORMATION

Corresponding Author

*E-mail: fabio.bellot@int.gov.br. Tel.: (55 21) 2123 1177. Fax: (55 21) 2123 1166.

Biographies



Lisiane V. Mattos received her B.S. degree from Federal University of Rio de Janeiro in 1993, M.Sc. degree in 1996, from COPPE/Federal University of Rio de Janeiro and Ph.D. degree in 2000 from COPPE/Federal University of Rio de Janeiro. She got a postdoctoral position in the Catalysis group of National Institute of Technology (INT) from 2000 to 2008. She is currently an assistant professor of Petroleum and Chemical Engineering Department at Fluminense Federal University. She has been involved in studies for the conversion of natural gas to syngas and fuels and the production of hydrogen from renewable sources, such as bioethanol, biomass, and water. Current research projects involve process intensification by using multifunctional reactors (membrane reactors, combining reaction and separation steps, or structured reactors like monoliths and plate reactors), development of SOFC anodes to energy generation from ethanol reforming, and solar-thermal water-splitting technologies.



Gary Jacobs was born in Newmarket, United Kingdom, in 1971. He received a B.S. in chemical engineering from University of Texas in 1993 and a Ph.D. in chemical engineering from University of Oklahoma in 2000, where he worked with Prof. Daniel E. Resasco on applying synchrotron techniques to the development of dehydrocyclization catalysts. He then joined the Davis group at University of Kentucky CAER. He has coauthored over 100 refereed publications and received, with Dr. Davis, four Elsevier

top-50 most-cited-author awards in catalysis for articles in cobalt-catalyzed Fischer–Tropsch synthesis and low-temperature water gas shift for fuel cell reformer applications.



Burtron H. Davis was born in Points, West Virginia, USA. He graduated with a B.S. in chemistry from West Virginia University in 1959 followed by a M.S. from St. Joseph's College (Philadelphia) and a Ph.D. from the University of Florida (Gainesville). This was followed by a postdoctoral position under Paul Emmett at Johns Hopkins from 1965–1966, and a period of research with Mobil R&D Corporation, where he worked on naphtha reforming and aromatics hydrogenation. He held the appointment of Associate Professor of Chemistry, Potomac State College, West Virginia, from 1970–1977. He then joined CAER and has directed the Clean Fuels and Chemicals (CFC) group since 1982. He has authored/coauthored over 600 publications and was awarded the prestigious Henry H. Storch award in Fuel Chemistry (2002) for his significant contributions in catalysis, Fischer–Tropsch synthesis, and coal conversion research.



Fabio B. Noronha received his B.S. degree from Federal University of Rio de Janeiro in 1987, M.Sc. degree in 1989 from COPPE/Federal University of Rio de Janeiro, and Ph.D. degree in 1994 from COPPE/Federal University of Rio de Janeiro and Institut des Recherches sur la Catalyse—Lyon/France. In 1996, he joined the Catalysis group of National Institute of Technology (INT). He worked in a postdoctoral position with Prof. Daniel Resasco at Oklahoma University from 1999–2000. He is interested in understanding the fundamental relationships between catalytic performance and the catalyst structure. He has been involved in studies for the conversion of natural gas to syngas and fuels, hydrogen and fuel production from biomass, including the steam reforming of ethanol and bio-oil and the gasification process. Current research projects involve process intensification by using multifunctional reactors such as membrane reactors, combining reaction and separation steps, or structured reactors like monoliths and plate reactors. He is the author or coauthor of around 270 technical publications.

ACKNOWLEDGMENTS

This work received financial support from CNPq and FINEP and the Commonwealth of Kentucky.

REFERENCES

- (1) Huber, G. W.; Iborra, S.; Corma, A. *Chem. Rev.* **2006**, *106*, 4044.
- (2) Haryanto, A.; Fernando, S.; Murali, N.; Adhikari, S. *Energy Fuels* **2005**, *19*, 2098.
- (3) Vaidya, P. D.; Rodrigues, A. E. *Chem. Eng. J.* **2006**, *117*, 39.
- (4) Ni, M.; Leung, Y. C.; Leung, M. K. H. *Int. J. Hydrogen Energy* **2007**, *32*, 3238.
- (5) de la Piscina, P. R.; Homs, N. *Chem. Soc. Rev.* **2008**, *37*, 2459.
- (6) Kugai, J.; Subramani, V.; Song, C. *Catal. Lett.* **2005**, *101*, 255.
- (7) Garcia, E. Y.; Laborde, M. A. *Int. J. Hydrogen Energy* **1991**, *16*, 307.
- (8) Vasudeva, K.; Mitra, N.; Umasankar, P.; Dhingra, S. C. *Int. J. Hydrogen Energy* **1996**, *21*, 13.
- (9) Fishtik, I.; Alexander, A.; Datta, R.; Geana, D. *Int. J. Hydrogen Energy* **2001**, *25*, 31.
- (10) Mas, V.; Kipreos, R.; Amadeo, N.; Laborde, M. *Int. J. Hydrogen Energy* **2006**, *31*, 21.
- (11) Semelsberger, T. A.; Brown, L. F.; Borup, R. L.; Inbody, M. A. *Int. J. Hydrogen Energy* **2004**, *29*, 1047.
- (12) Rabenstein, G.; Hacker, V. *J. Power Sources* **2008**, *185*, 1293.
- (13) Liu, S.; Zhang, K.; Fang, L.; Y. Li, Y. *Energy Fuels* **2008**, *22*, 1365.
- (14) Fatsikostas, A. N.; Kondarides, D. I.; Verykios, X. E. *Chem. Commun.* **2001**, 851.
- (15) Fatsikostas, A. N.; Verykios, X. E. *J. Catal.* **2004**, *225*, 439.
- (16) Fatsikostas, A. N.; Kondarides, D. I.; Verykios, X. E. *Catal. Today* **2002**, *75*, 145.
- (17) Klouz, V.; Fierro, V.; Denton, P.; Katz, H.; Lisse, J. P.; Bouvot-Mauduit, S.; Mirodatos, C. *J. Power Sources* **2002**, *105*, 26.
- (18) Fierro, V.; Klouz, V.; Akdim, O.; Mirodatos, C. *Catal. Today* **2002**, *75*, 141.
- (19) Fierro, V.; Akdim, O.; Mirodatos, C. *Green Chem.* **2003**, *5*, 20.
- (20) Velu, S.; Satoh, N.; Gopinath, C. S.; Suzuki, K. *Catal. Lett.* **2002**, *82*, 145.
- (21) Liguras, D. K.; Kondarides, D. I.; Verykios, X. E. *Appl. Catal., B* **2003**, *43*, 345.
- (22) Goula, M. A.; Kontou, S.; Zhou, W.; Qin, X.; Tsakarlas, P. E. *Ionics* **2003**, *9*, 248.
- (23) Goula, M. A.; Kontou, S.; Tsakarlas, P. E. *Appl. Catal., B* **2004**, *49*, 135.
- (24) Fierro, V.; Akdim, O.; Provendier, H.; Mirodatos, C. *J. Power Sources* **2005**, *145*, 6596.
- (25) Haga, F.; Nakajima, T.; Miya, H.; Mishima, S. *Catal. Lett.* **1997**, *48*, 223.
- (26) Zhang, B.; Tang, X.; Li, Y.; Cai, W.; Xu, Y.; Shen, W. *Catal. Commun.* **2006**, *7*, 367.
- (27) Biswas, P.; Kunzru, D. *Int. J. Hydrogen Energy* **2007**, *32*, 969.
- (28) Vizcaino, A. J.; Carrero, A.; Calles, J. A. *Int. J. Hydrogen Energy* **2007**, *32*, 1450.
- (29) Song, H.; Zhang, L.; Watson, R. B.; Braden, D.; Ozkan, U. S. *Catal. Today* **2007**, *129*, 346.
- (30) Montini, T.; de Rogatis, L.; Gombac, V.; Fornasiero, P.; Graziani, M. *Appl. Catal., B* **2007**, *71*, 125.
- (31) Domok, M.; Tóth, M.; Raskó, J.; Erdőhelyi, A. *Appl. Catal., B* **2007**, *69*, 262.
- (32) Deluga, G. A.; Salge, J. R.; Schmidt, L. D.; Verykios, X. E. *Science* **2004**, *303*, 993.
- (33) Cavallaro, S.; Chiodo, V.; Freni, S.; Mondello, N.; Frusteri, F. *Appl. Catal., A* **2003**, *249*, 119.
- (34) Comas, J.; Marino, F.; Laborde, M.; Amadeo, N. *Chem. Eng. J.* **2004**, *98*, 61.
- (35) Wanat, E. C.; Venkataraman, K.; Schmidt, L. D. *Appl. Catal., A* **2004**, *276*, 155.

- (36) Cai, W.; Wang, F.; Zhan, E.; van Veen, A. C.; Mirodatos, C.; Shen, W. *J. Catal.* **2008**, *257*, 96.
- (37) de Lima, S. M.; da Cruz, I. O.; Jacobs, G.; Davis, B. H.; Mattos, L. V.; Noronha, F. B. *J. Catal.* **2008**, *257*, 356.
- (38) de Lima, S. M.; da Silva, A. M.; da Costa, L. O. O.; Jacobs, G.; Davis, B. H.; Mattos, L. V.; Noronha, F. B. *J. Catal.* **2009**, *268*, 268.
- (39) de Lima, S. M.; da Silva, A. M.; Graham, U. M.; Jacobs, G.; Davis, B. H.; Mattos, L. V.; Noronha, F. B. *Appl. Catal., A* **2009**, *352*, 95.
- (40) de Lima, S. M.; da Silva, A. M.; da Costa, L. O. O.; Assaf, J. M.; Jacobs, G.; Davis, B. H.; Mattos, L. V.; Noronha, F. B. *Appl. Catal., A* **2010**, *377*, 181.
- (41) Cavallaro, S.; Mondelo, N.; Freni, S. *J. Power Source* **2001**, *102*, 198.
- (42) da Silva, A. M.; da Costa, L. O. O.; Souza, K. R.; Mattos, L. V.; Noronha, F. B. *Catal. Commun.* **2010**, *11*, 736.
- (43) Auprêtre, F.; Descorme, C.; Duprez, D. *Catal. Commun.* **2002**, *3*, 263.
- (44) Frusteri, F.; Freni, S.; Spadaro, L.; Chiodo, V.; Bonura, G.; Donato, S.; Cavallaro, S. *Catal. Commun.* **2004**, *5*, 611.
- (45) Basagiannis, A. C.; Panagiotopoulou, P.; Verykios, X. E. *Top. Catal.* **2008**, *51*, 2.
- (46) Breen, J. P.; Burch, R.; Coleman, H. M. *Appl. Catal., B* **2002**, *39*, 65.
- (47) Duan, S.; Senkan, S. *Ind. Eng. Chem. Res.* **2005**, *44*, 6381.
- (48) Szijjarto, G. P.; Tompos, A.; Margitfavi, J. L. *Appl. Catal., A* **2011**, *391*, 417.
- (49) Davda, R. R.; Shabaker, J. W.; Huber, G. W.; Cortright, R. D.; Dumesic, J. A. *Appl. Catal., B* **2005**, *56*, 171.
- (50) Cruz, I. O.; Ribeiro, N. F. P.; Aranda, A. G.; Souza, M. V. M. *Catal. Commun.* **2008**, *9*, 2606.
- (51) Tokarev, A. V.; Kirilin, A. V.; Murzina, E. V.; Eranen, K.; Kustov, L. M.; Murzin, D. Y.; Mikkola, J. P. *Int. J. Hydrogen Energy* **2010**, *35*, 12642.
- (52) Byrd, A. J.; Pant, K. K.; Gupta, R. B. *Energy Fuels* **2007**, *21*, 3541.
- (53) Rabe, S.; Nachtegaal, M.; Ulrich, T.; Vogel, F. *Angew. Chem., Int. Ed.* **2010**, *49*, 6434.
- (54) Voll, F. A. P.; Rossi, C. C. R. S.; Silva, C.; Guirardello, R.; Souza, R. O. M. A.; Cabral, V. F.; Cardozo-Filho, L. *Int. J. Hydrogen Energy* **2009**, *34*, 9737.
- (55) Bower, M.; Holroyd, R. P.; Sharpe, R. G.; Corneille, J. S.; Francis, S. M.; Goodman, D. W. *Surf. Sci.* **1997**, *370*, 113.
- (56) Shekhar, R.; Barreau, M. A.; Plank, R. V.; Vohs, J. M. *J. Phys. Chem. B* **1997**, *101*, 7939.
- (57) Lee, A. F.; Gawthrop, D. E.; Hart, N. J.; Wilson, K. *Surf. Sci.* **2004**, *548*, 200.
- (58) Mavrikakis, M.; Barreau, M. A. *J. Mol. Catal. A: Chem.* **1998**, *131*, 135.
- (59) Davis, J. L.; Barreau, M. A. *Surf. Sci.* **1997**, *235*, 113.
- (60) Cong, Y.; van Spaendonk, V.; Masel, R. I. *Surf. Sci.* **1997**, *385*, 246.
- (61) Gursahani, K. I.; Alcala, R.; Cortright, R. D.; Dumesic, J. A. *Appl. Catal., A* **2001**, *222*, 369.
- (62) Ferrin, P.; Simonetti, D.; Kandoi, S.; Kunkes, E.; Dumesic, J. A.; Nørskov, J. K.; Mavrikakis, M. *J. Am. Chem. Soc.* **2009**, *131*, 5809.
- (63) Alcala, J. R.; Mavrikakis, M.; Dumesic, J. A. *J. Catal.* **2003**, *218*, 178.
- (64) Alcala, R.; Shabaker, J. W.; Huber, G. W.; Sanchez-Castillo, M. A.; Dumesic, J. A. *J. Phys. Chem. B* **2005**, *109*, 2074.
- (65) Orest, S.; Barreau, M. A.; Jingguang, G. C. *Surf. Sci.* **2008**, *602*, 3578.
- (66) Yee, A.; Morrison, S. J.; Idriss, H. *J. Catal.* **2000**, *191*, 30.
- (67) Lee, W. T.; Thomas, F.; Masel, R. I. *Surf. Sci.* **1998**, *418*, 479.
- (68) Zhao, H.; Kim, J.; Koel, B. E. *Surf. Sci.* **2003**, *538*, 147.
- (69) Weststrate, C. J.; Ludwig, W.; Bakker, J. W.; Gluhoi, A. C.; Nieuwenhuys, B. E. *ChemPhysChem* **2007**, *8*, 932.
- (70) Idriss, H.; Diagne, C.; Hindermann, J. P.; Kiennemann, A.; Barreau, M. A. *J. Catal.* **1995**, *155*, 219.
- (71) Yee, A.; Morrison, S. J.; Idriss, H. *J. Catal.* **1999**, *186*, 279.
- (72) Yee, A.; Morrison, S. J.; Idriss, H. *Catal. Today* **2000**, *63*, 327.
- (73) Sheng, P. Y.; Yee, A.; Bowmaker, G. A.; Idriss, H. *J. Catal.* **2002**, *208*, 393.
- (74) Raskó, J.; Hancz, A.; Erdőhelyi, A. *Appl. Catal., A* **2004**, *269*, 13.
- (75) Raskó, J.; Kiss, J. *Catal. Lett.* **2005**, *101*, 71.
- (76) Erdőhelyi, A.; Raskó, J.; Kecskés, T.; Tóth, M.; Dömök, M.; Baán, K. *Catal. Today* **2006**, *116*, 367.
- (77) Raskó, J.; Dömök, M.; Baán, K.; Erdőhelyi, A. *Appl. Catal., A* **2006**, *299*, 202.
- (78) Dömök, M.; Baán, K.; Kecskés, T.; Erdőhelyi, A. *Catal. Lett.* **2008**, *126*, 49.
- (79) Song, H.; Ozkan, U. S. *J. Phys. Chem. A* **2010**, *114*, 3796.
- (80) Song, H.; Ozkan, U. S. *J. Catal.* **2009**, *261*, 66.
- (81) Guil, J. M.; Hom, N.; Llorca, J.; de la Piscina, P. R. *J. Phys. Chem. B* **2005**, *109*, 10813.
- (82) Mattos, L. V.; Noronha, F. B. *J. Catal.* **2005**, *233*, 453.
- (83) Mattos, L. V.; Noronha, F. B. *Power Sources* **2005**, *152*, 50.
- (84) Silva, A. M.; Costa, L. O. O.; Barandas, A. P. M. G.; Borges, L. E. P.; Mattos, L. V.; Noronha, F. B. *Catal. Today* **2008**, *133*, 755.
- (85) El-Maazawi, M.; Finken, A. N.; Nair, A. B.; Grassian, V. H. *J. Catal.* **2000**, *191*, 138.
- (86) Takanabe, K.; Aika, K.; Seshan, K.; Lefferts, L. *J. Catal.* **2004**, *227*, 101.
- (87) Baldanza, M. A. S.; de Mello, L. F.; Vannice, A.; Noronha, F. B.; Schmal, M. *J. Catal.* **2000**, *192*, 64.
- (88) Cordi, E. M.; Falconer, J. L. *J. Catal.* **1996**, *162*, 104.
- (89) de Mello, L. F.; Noronha, F. B.; Schmal, M. *J. Catal.* **2003**, *220*, 358.
- (90) Di Cosimo, J. I.; Diez, V. K.; Xu, M.; Iglesia, E.; Apesteguia, C. R. *J. Catal.* **1998**, *178*, 499.
- (91) Takahara, I.; Saito, M.; Inaba, M.; Murata, K. *Catal. Lett.* **2005**, *105*, 249.
- (92) Inaba, M.; Murata, K.; Saito, M.; Takahara, I. *React. Kinet. Catal. Lett.* **2006**, *88*, 135.
- (93) Di Cosimo, J. I.; Apesteguia, C. R.; Gines, M. J. L.; Iglesia, E. *J. Catal.* **2000**, *190*, 261.
- (94) Llorca, J.; Hom, N.; de la Piscina, P. R. *J. Catal.* **2004**, *227*, 556.
- (95) Lin, S. S.-Y.; Kim, D. H.; Ha, S. Y. *Appl. Catal., A* **2009**, *355*, 69.
- (96) Jacobs, G.; Keogh, R. A.; Davis, B. H. *J. Catal.* **2007**, *245*, 326.
- (97) de Lima, S. M.; Colman, R. C.; Jacobs, G.; Davis, B. H.; Souza, K. R.; de Lima, A. F. F.; Appel, L. G.; Mattos, L. V.; Noronha, F. B. *Catal. Today* **2009**, *146*, 110.
- (98) de Lima, S. M.; Silva, A. M.; da Cruz, I. O.; Jacobs, G.; Davis, B. H.; Mattos, L. V.; Noronha, F. B. *Catal. Today* **2008**, *138*, 162.
- (99) Akdim, O.; Cai, W.; Fierro, V.; Provendier, H.; Van Veen, A.; Shen, W.; Mirodatos, C. *Top. Catal.* **2008**, *51*, 22.
- (100) Roh, H.; Platon, A.; Wang, Y.; King, D. L. *Catal. Lett.* **2006**, *110*, 1.
- (101) Platon, A.; Roh, H. S.; King, D. L.; Wang, Y. *Top. Catal.* **2007**, *46*, 374.
- (102) Vargas, J. C.; Libs, S.; Roger, A. C.; Kiennemann, A. *Catal. Today* **2005**, *107*, 417.
- (103) Galetti, A. E.; Gomez, M. F.; Arrua, L. A.; Marchi, A. J.; Abello, M. C. *Catal. Commun.* **2008**, *9*, 1201.
- (104) Wang, H.; Liu, Y.; Wang, L.; Qin, Y. N. *Chem. Eng. J.* **2008**, *145*, 25.
- (105) Romero-Sarria, F.; Vargas, J. C.; Roger, A.; Kiennemann, A. *Catal. Today* **2008**, *133*, 149.
- (106) Frusteri, F.; Freni, S.; Chiodo, V.; Donato, S.; Bonura, G.; Cavallaro, S. *Int. J. Hydrogen Energy* **2006**, *31*, 2193.
- (107) Trimm, D. L. *Catal. Today* **1999**, *49*, 3.
- (108) Roh, Y. H.; Wang, D. L.; King, D. L.; Chin, Y. H. *Catal. Lett.* **2006**, *108*, 15.
- (109) Guiñet, M.; Magnoux, P. *Appl. Catal.* **1989**, *54*, 1.
- (110) Bartholomew, C. H.; Farrauto, R. J. In *Fundamentals of Industrial Catalytic Process*, 2nd ed.; John Wiley & Sons: New Jersey, 2006; p 654.
- (111) Mattos, L. V.; Noronha, F. B.; Monteiro, J. L. F. *J. Catal.* **2002**, *209*, 166.

- (112) Iglesia, E.; Barton, D. G.; Biscardi, J. A.; Gines, M. J. L.; Soled, S. L. *Catal. Today* **1997**, *38*, 339.
- (113) Rostrup-Nielsen, J. R. *Catal. Today* **1993**, *18*, 305.
- (114) Rostrup-Nielsen, J. R.; Rostrup-Nielsen, T. *CATTECH* **2002**, *6*, 150.
- (115) Rostrup-Nielsen, J. R.; Sehested, J.; Norskov, J. *Adv. Catal.* **2002**, *47*, 65.
- (116) Takehira, K.; Ohi, T.; Shishido, T.; Kawabata, T.; Takaki, K. *Appl. Catal., A* **2005**, *283*, 137.
- (117) Park, C.; Keane, M. A. *J. Catal.* **2004**, *221*, 386.
- (118) Savva, P. G.; Polychronopoulou, K.; Ryzkov, V. A.; Efstatiou, A. M. *Appl. Catal., B* **2010**, *93*, 314.
- (119) Jones, G.; Jakobsen, J.G. J.G.; Shim, S. S.; Kleis, J.; Andersson, M. P.; Rossmeisl, J.; Abild-Pedersen, F.; Bligaard, T.; Helveg, S.; Hinnemann, B.; Rostrup-Nielsen, J. R.; Chorkendorff, I.; Sehested, J.; Norskov, J. K. *J. Catal.* **2008**, *259*, 147.
- (120) Wei, J.; Iglesia, E. *J. Phys. Chem. B* **2004**, *108*, 4094.
- (121) Rostrup-Nielsen, J. P.; Hansen, J. H. B. *J. Catal.* **1993**, *144*, 38.
- (122) Qin, D.; Lapszewicz, J. *Catal. Today* **1994**, *21*, 551.
- (123) Palmeri, N.; Cavallaro, S.; Chiodo, V.; Freni, S.; Frusteri, F.; Bart, J. C. *J. Int. J. Hydrogen Energy* **2007**, *32*, 3335.
- (124) Frusteri, F.; Freni, S. *J. Power Sources* **2007**, *173*, 200.
- (125) Dömöök, M.; Oszko, A.; Baán, K.; Sarusi, I.; Erdőhelyi, A. *Appl. Catal., A* **2010**, *383*, 33.
- (126) Takanabe, K.; Aika, K.; Inazu, K.; Baba, T.; Seshan, K.; Lefferts, L. *J. Catal.* **2006**, *243*, 263.
- (127) Llorca, J.; Homs, N.; Sales, J.; de la Piscina, P. R. *J. Catal.* **2002**, *209*, 306.
- (128) Jeong, N.; Lee, J. *J. Catal.* **2008**, *260*, 217.
- (129) Diao, J.; Wang, H.; Li, W.; Wang, G.; Ren, Z.; Bai, J. *Physica E* **2010**, *42*, 2280.
- (130) Bichon, P.; Haugom, G.; Venvik, H. J.; Holmen, A.; Blekkan, E. A. *Top. Catal.* **2008**, *49*, 38.
- (131) Trimm, D. L. *Catal. Today* **1997**, *37*, 233.
- (132) Sanchez-Sanchez, M. C.; Yerga, R. M. N.; Kondarides, D. I.; Verykios, X. E.; Fierro, J. L. G. *J. Phys. Chem. A* **2010**, *114* (11), 3873.
- (133) Kugai, J.; Velu, S.; Song, C.; Engelhard, M. H.; Chin, Y. *J. Catal.* **2006**, *238*, 430.
- (134) Virginie, M.; Araque, M.; Roger, A. C.; Vargas, J. C.; Kiennemann, A. *Catal. Today* **2008**, *138*, 21.
- (135) Sun, C.; Stimming, U. *J. Power Sources* **2007**, *171*, 247.
- (136) Laosiripojana, N.; Assabumrungrat, S. *J. Power Sources* **2007**, *163*, 943.
- (137) Cimenti, M.; Hill, J. M. *J. Power Sources* **2009**, *186*, 377.
- (138) Ye, X.-F.; Huang, B.; Wang, S. R.; Wang, Z. R.; Xiong, L.; Wen, T. L. *J. Power Sources* **2007**, *164*, 203.
- (139) Cimenti, M.; Hill, J. M. *J. Power Sources* **2010**, *195*, 3996.
- (140) Huang, B.; Wang, S. R.; Liu, R. Z.; Wen, T. L. *J. Power Sources* **2007**, *167*, 288.
- (141) Ye, X.-F.; Wang, S. R.; Wang, Z. R.; Xiong, L.; Sun, X. F.; Wen, T. L. *J. Power Sources* **2008**, *177*, 419.
- (142) Ye, X.-F.; Wang, S. R.; Hu, Q.; Chen, J. Y.; Wen, T. L.; Wen, Z. Y. *Solid State Ionics* **2009**, *180*, 276.
- (143) Cela, B.; Macedo, D. A.; Souza, G. L.; Martinelli, A.E., R.; Nascimento, R. M.; Paskocimas, C. A. *J. Power Sources* **2011**, *196*, 2539.
- (144) le Valant, A.; Garron, A.; Bion, N.; Epron, F.; Duprez, D. *Catal. Today* **2008**, *138*, 169.
- (145) Rass-Hansen, J.; Johansson, R.; Moller, M.; Christensen, C. H. *Int. J. Hydrogen Energy* **2008**, *33*, 4547.
- (146) Akande, A. J.; Idem, R. O.; Dalai, A. K. *Appl. Catal., A* **2005**, *287*, 159.
- (147) Laosiripojana, N.; Assabumrungrat, S. *Appl. Catal., A* **2007**, *327*, 180.
- (148) Pereira, E. B.; Homs, N.; Marti, S.; Fierro, J. L. G.; de la Piscina, P. R. *J. Catal.* **2008**, *257*, 206.
- (149) Velu, S.; Suzuki, K.; Vijayaraj, M.; Barman, S.; Gopinath, C. S. *Appl. Catal., B* **2005**, *55*, 287.
- (150) Navarro, R. M.; Alvarez-Galvan, M. C.; Cruz Sanchez-Sanchez, M.; Rosa, F.; Fierro, J. L. G. *Appl. Catal., B* **2005**, *55*, 229.
- (151) Cai, W.; Wanga, F.; van Veen, A. C.; Provendier, H.; Mirodatos, C.; Shen, W. *Catal. Today* **2008**, *138*, 152.
- (152) Biswas, P.; Kunzru, D. *Catal. Lett.* **2007**, *118*, 36.
- (153) Bi, J. L.; Hong, Y. Y.; Lee, C. C.; Yeh, C. T.; Wang, C. B. *Catal. Today* **2007**, *129*, 322.
- (154) Huang, L.; Xie, J.; Chen, R.; Chu, D.; Hsu, A. T. *Mater. Res. Bull.* **2010**, *45*, 92.
- (155) Youn, M. H.; Seo, J. G.; Kim, P.; Song, I. K. *J. Mol. Catal. A* **2007**, *261*, 276.
- (156) Cavallaro, S.; Chiodo, V.; Vita, A.; Freni, S. *J. Power Sources* **2003**, *123*, 10.
- (157) Mattos, L. V.; Noronha, F. B. *J. Power Sources* **2005**, *145*, 10.
- (158) Silva, A. M.; Costa, L. O. O.; Barandas, A. P. M. G.; Borges, L. E. P.; Mattos, L. V.; Noronha, F. B. *Catal. Today* **2007**, *129*, 297.
- (159) Costa, L. O. O.; Silva, A. M.; Borges, L. E. P.; Mattos, L. V.; Noronha, F. B. *Catal. Today* **2008**, *138*, 147.
- (160) Bi, J. L.; Hsu, S. N.; Yeh, C. T.; Wang, C. B. *Catal. Today* **2007**, *129*, 330.
- (161) Weng, W.; Wang, Z.; Ding, Y.; Xu, J.; Lu, G. *Catal. Lett.* **2002**, *81*, 63.
- (162) Silva, A. M.; de Farias, A. M. D.; Costa, L. O. O.; Barandas, A. P. M. G.; Mattos, L. V.; Fraga, M. F.; Noronha, F. B. *Appl. Catal., A* **2008**, *334*, 179.
- (163) Galetti, A. E.; Gomez, M. F.; Arrua, L. A.; Abello, M. C. *Appl. Catal., A* **2008**, *348*, 94.
- (164) de Lima, S. M.; da Silva, A. M.; Jacobs, G.; Davis, B. H.; Mattos, L. V.; Noronha, F. B. *Appl. Catal., B* **2010**, *96*, 387.
- (165) Jankhah, S.; Abatzoglou, N.; Gitzhofer, F. *Int. J. Hydrogen Energy* **2008**, *33*, 4769.
- (166) Bellido, J. D. A.; Tanabe, E. Y.; Assaf, E. M. *Appl. Catal., B* **2009**, *90*, 485.
- (167) da Silva, A. M.; de Souza, K. R.; Jacobs, G.; Graham, U. M.; Davis, B. H.; Mattos, L. V.; Noronha, F. B. *Appl. Catal., B* **2011**, *102*, 94.
- (168) Llorca, J.; Homs, N.; Sales, J.; Fierro, J. L. G.; de la Piscina, P. R. *J. Catal.* **2004**, *222*, 470.
- (169) Frusteri, F.; Freni, S.; Chiodo, V.; Spadaro, L.; di Blasi, O.; Bonura, G.; Cavallaro, S. *Appl. Catal., A* **2004**, *270*, 1.
- (170) Carrero, A.; Calles, J. A.; Vizcaino, A. J. *Chem. Eng. J.* **2010**, *163*, 395.
- (171) Liberatori, J. W. C.; Ribeiro, R. U.; Zanchet, D.; Noronha, F. B.; Bueno, J. M. C. *Appl. Catal., A* **2007**, *327*, 197.
- (172) Sanchez-Sanchez, M. C.; Navarro, R. M.; Fierro, J. L. G. *Int. J. Hydrogen Energy* **2007**, *32*, 1462.
- (173) Sanchez-Sanchez, M. C.; Navarro, R. M.; Fierro, J. L. G. *Catal. Today* **2007**, *129*, 336.
- (174) Can, F.; le Valant, A.; Bion, N.; Epron, F.; Duprez, D. *J. Phys. Chem. C* **2008**, *112*, 14145.
- (175) Llorca, J.; de la Piscina, P. R.; Dalmon, J. A.; Sales, J.; Homs, N. *Appl. Catal., B* **2003**, *43*, 355.
- (176) Roh, H. S.; Wang, Y.; King, D. L. *Top. Catal.* **2008**, *49*, 32.
- (177) Lin, S. S. Y.; Daimon, H.; Ha, S. Y. *Appl. Catal., A* **2009**, *366*, 252.
- (178) Song, H.; Tan, B.; Ozkan, U. S. *Catal. Lett.* **2009**, *132*, 132.
- (179) Nishiguchi, T.; Matsumoto, T.; Kanai, H.; Utani, K.; Matsumura, Y.; Shen, W. J.; Imamura, S. *Appl. Catal., A* **2005**, *279*, 273.
- (180) Wang, H.; Ye, J. L.; Liu, Y.; Li, Y. D.; Qin, Y. N. *Catal. Today* **2007**, *129*, 305.
- (181) Sheng, P. Y.; Chiu, W. W.; Yee, A.; Morrison, S. J.; Idriss, H. *Catal. Today* **2007**, *129*, 313.
- (182) Cai, W.; Zhang, B.; Li, Y.; Xu, Y.; Shen, W. *Catal. Commun.* **2007**, *8*, 1588.
- (183) da Silva, A. M.; de Souza, K. R.; Mattos, L. V.; Jacobs, G.; Davis, B. H.; Noronha, F. B. *Catal. Today* **2011**, *164*, 234.
- (184) Furtado, A. C.; Alonso, C. G.; Cantão, M. P.; Fernandes-Machado, N. R. C. *Int. J. Hydrogen Energy* **2009**, *34*, 7189.

- (185) Kaspar, J.; Fornasiero, P.; Graziani, M. *Catal. Today* **1999**, *50*, 285.
- (186) Homs, N.; Llorca, J.; de la Piscina, P. R. *Catal. Today* **2008**, *133*, 149.
- (187) Rostrup-Nielsen, J. R. *J. Catal.* **1984**, *85*, 31.
- (188) da Silva, A.L. M.; Mattos, L. V.; von Breen, J.; Bitter, J. H.; de Jong, K. P.; Noronha, F. B., eds. *Book of abstracts of NGCS 9*, Lyon, France, 2010; paper KN06.
- (189) Mas, V.; Dieuzeide, M. L.; Jobbagy, M.; Baronetti, G.; Amadeo, N.; Laborde, M. *Chem. Eng. J.* **2008**, *138*, 602.
- (190) Bussi, J.; Bespalko, N.; Veiga, S.; Amaya, A.; Faccio, R.; Abello, M. C. *Catal. Commun.* **2008**, *10*, 33.
- (191) Chica, A.; Sayas, S. *Catal. Today* **2009**, *146*, 37.
- (192) Vizcaino, A. J.; Carrero, A.; Calles, J. A. *Int. J. Hydrogen Energy* **2007**, *32*, 1450.
- (193) Seelam, P. K.; Huuhtanen, M.; Sapi, A.; Szabo, M.; Kordas, K.; Turpeinen, E.; Toth, G.; Keiski, R. L. *Int. J. Hydrogen Energy* **2010**, *35*, 12588.
- (194) Barthos, R.; Szechenyi, A.; Solymosi, F. *Catal. Lett.* **2008**, *120*, 161.
- (195) Mas, V.; Baronetti, G.; Amadeo, N.; Laborde, M. *Chem. Eng. J.* **2008**, *138*, 602.
- (196) Romero, A.; Jobbagy, M.; Laborde, M.; Baronetti, G.; Amadeo, N. *Catal. Today* **2010**, *149*, 407.
- (197) Guil-Lopez, R.; Navarro, R. M.; Pena, M. A.; Fierro, J. L. G. *Int. J. Hydrogen Energy* **2011**, *36*, 1512.
- (198) He, L.; Berntsen, H.; Ocho-Fernandez, E.; Walmsley, J. C.; Blekkan, E. A.; Chen, D. *Top. Catal.* **2009**, *52*, 206.
- (199) Li, M.; Wang, X.; Li, S.; Wang, S.; Ma, X. *Int. J. Hydrogen Energy* **2010**, *35*, 6699.
- (200) Venugopal, A.; Sudhakar, M.; Kishore, R.; Reema Sarkari, J.; Ashok, S. M.; de Lima, F. B.; Noronha, A. H.; Padmasri. *Int. J. Nanotechnol.* **2010**, *7*, 1188.
- (201) Valderrama, G.; Goldwasser, M. R.; de Navarro, C. U.; Tatibouë, J. M.; Barrault, J.; Batiot-Dupeyrat, C.; Martínez, F. *Catal. Today* **2005**, *107*, 785.
- (202) Lima, S. M.; Assaf, J. M.; Peña, M. A.; Fierro, J. L. G. *Appl. Catal., A* **2006**, *311*, 94.
- (203) Chen, H.; Yu, H.; Peng, F.; Yang, G.; Wang, H.; Yang, J.; Tang, Y. *Chem. Eng. J.* **2010**, *160*, 333.
- (204) Liu, J. Y.; Lee, C. C.; Wang, C. H.; Yeh, C. T.; Wang, C. B. *Int. J. Hydrogen Energy* **2010**, *35*, 4069.
- (205) Pena, M. A.; Fierro, J. L. G. *Chem. Rev.* **2001**, *101*, 1981.
- (206) Ribeiro, R. U.; Liberatori, W. C.; Winnishofer, H.; Bueno, J. M. C.; Zanchet, D. *Appl. Catal., B* **2009**, *91*, 670.
- (207) Beltramini, J.; Trimm, D. L. *Appl. Catal.* **1983**, *32*, 149.
- (208) Haller, G. L.; Resasco, D. *Adv. Catal.* **1989**, *36*, 173.
- (209) Youn, M. H.; Seo, J. G.; Kim, P.; Song, I. K. *J. Mol. Catal. A* **2007**, *261*, 276.
- (210) de la Pena O'Shea, V. A.; Homs, N.; Pereira, E. B.; Nafria, R.; de la Piscina, P. R. *Catal. Today* **2007**, *126*, 148.
- (211) da Silva, A.L. M.; Mattos, L. V.; den Breejen, J. P.; Bitter, J. H.; de Jong, K. P.; Noronha, F. B. *Catal. Today* **2011**, *164*, 262.